A&A 595, A133 (2016)
DOI: 10.1051/0004-6361/201629583

Astronomy & Astrophysics
Special issue

Gaia Data Release 1

Gaia Data Release 1

The Cepheid and RR Lyrae star pipeline and its application to the south ecliptic pole region⋆

G. Clementini[1,⋆⋆], V. Ripepi[2], S. Leccia[2], N. Mowlavi[3], I. Lecoeur-Taibi[4], M. Marconi[2], L. Szabados[5], L. Eyer[3], L. P. Guy[4], L. Rimoldini[4], G. Jevardat de Fombelle[6], B. Holl[4], G. Busso[7], J. Charnas[4], J. Cuypers[8], F. De Angeli[7], J. De Ridder[9], J. Debosscher[9], D. W. Evans[7], P. Klagyivik[5], I. Musella[2], K. Nienartowicz[6], D. Ordóñez[4], S. Regibo[9], M. Riello[7], L. M. Sarro[10], and M. Süveges[4]

[1] INAF−Osservatorio Astronomico di Bologna, via Ranzani 1, 40127 Bologna, Italy
[2] INAF−Osservatorio Astronomico di Capodimonte, Salita Moiariello 16, 80131 Napoli, Italy
[3] Department of Astronomy, University of Geneva, Ch. des Maillettes 51, 1290 Versoix, Switzerland
[4] Department of Astronomy, University of Geneva, Ch. d'Ecogia 16, 1290 Versoix, Switzerland
[5] Konkoly Observatory, Research Centre for Astronomy and Earth Sciences, Hungarian Academy of Sciences, 1121 Budapest, Konkoly Thege M. ut 15-17, Hungary
[6] SixSq, Rue du Bois-du-Lan 8, 1217 Geneva, Switzerland
[7] Institute of Astronomy, University of Cambridge, Madingley Road, Cambridge CB3 0HA, UK
[8] Royal Observatory of Belgium, Ringlaan 3, 1180 Brussels, Belgium
[9] Institute of Astronomy, KU Leuven, Celestijnenlaan 200D, 3001 Leuven, Belgium
[10] Dpto. Inteligencia Artificial, UNED, c/ Juan del Rosal 16, 28040 Madrid, Spain

Received 25 August 2016 / Accepted 11 October 2016

ABSTRACT

Context. The European Space Agency spacecraft *Gaia* is expected to observe about 10 000 Galactic Cepheids and over 100 000 Milky Way RR Lyrae stars (a large fraction of which will be new discoveries), during the five-year nominal lifetime spent scanning the whole sky to a faint limit of $G = 20.7$ mag, sampling their light variation on average about 70 times.
Aims. We present an overview of the Specific Objects Study (SOS) pipeline developed within the Coordination Unit 7 (CU7) of the Data Processing and Analysis Consortium (DPAC), the coordination unit charged with the processing and analysis of variable sources observed by *Gaia*, to validate and fully characterise Cepheids and RR Lyrae stars observed by the spacecraft. The algorithms developed to classify and extract information such as the pulsation period, mode of pulsation, mean magnitude, peak-to-peak amplitude of the light variation, subclassification in type, multiplicity, secondary periodicities, and light curve Fourier decomposition parameters, as well as physical parameters such as mass, metallicity, reddening, and age (for classical Cepheids) are briefly described.
Methods. The full chain of the CU7 pipeline was run on the time series photometry collected by *Gaia* during 28 days of ecliptic pole scanning law (EPSL) and over a year of nominal scanning law (NSL), starting from the general Variability Detection, general Characterization, proceeding through the global Classification and ending with the detailed checks and typecasting of the SOS for Cepheids and RR Lyrae stars (SOS Cep&RRL). We describe in more detail how the SOS Cep&RRL pipeline was specifically tailored to analyse *Gaia*'s *G*-band photometric time series with a south ecliptic pole (SEP) footprint, which covers an external region of the Large Magellanic Cloud (LMC), and to produce results for confirmed RR Lyrae stars and Cepheids to be published in *Gaia* Data Release 1 (*Gaia* DR1).
Results. *G*-band time series photometry and characterisation by the SOS Cep&RRL pipeline (mean magnitude and pulsation characteristics) are published in *Gaia* DR1 for a total sample of 3194 variable stars (599 Cepheids and 2595 RR Lyrae stars), of which 386 (43 Cepheids and 343 RR Lyrae stars) are new discoveries by *Gaia*. All 3194 stars are distributed over an area extending 38 degrees on either side from a point offset from the centre of the LMC by about 3 degrees to the north and 4 degrees to the east. The vast majority are located within the LMC. The published sample also includes a few bright RR Lyrae stars that trace the outer halo of the Milky Way in front of the LMC.

Key words. stars: general – stars: oscillations – stars: variables: Cepheids – stars: variables: RR Lyrae – methods: data analysis – Magellanic Clouds

⋆ The full atlas of light curves is available at http://davide2.bo.astro.it/~felix/
⋆⋆ Corresponding author: G. Clementini, e-mail: gisella.clementini@oabo.inaf.it

1. Introduction

Easy to recognise thanks to their characteristic light variation, Cepheids and RR Lyrae stars are radial pulsating variables that trace stellar populations with different age and chemical composition: classical Cepheids (hereafter DCEPs) trace a young ($t \lesssim 300$ Myr) stellar component; anomalous Cepheids (ACEPs) can trace stars of intermediate age ($t \sim 1$–5 Gyr) and metal poor content ([Fe/H] < -1.5 dex), although it is still matter of debate whether they might also arise from coalescence of binary stars as old as about 10 Gyr; finally, the RR Lyrae stars and the Type II Cepheids (T2CEPs) trace an old ($t > 10$ Gyr) stellar population.

They are primary standard candles in establishing the cosmic distance ladder because Cepheids conform to period-luminosity (*PL*), period-luminosity-colour (*PLC*), and period-Wesenheit (*PW*) relations, whereas the RR Lyrae stars follow a luminosity-metallicity relation in the visual band (M_V–[Fe/H]) and a period-luminosity-metallicity (*PLZ*) relation in the infrared.

With its multi-epoch monitoring of the full sky, *Gaia* will discover and measure position, parallax, proper motion and time series photometry of thousands of Cepheids and RR Lyrae stars in the Milky Way (MW) and its surroundings down to a faint magnitude limit of $G \sim 20.7$ mag. The spacecraft is expected to observe from 2000 to 9000 MW Cepheids, about 70 000 RR Lyrae stars in the Galactic halo, from 15 000 to 40 000 RR Lyrae in the MW bulge (see Table 3 in Eyer et al. 2012, and references therein), and according to the most recent estimates (Soszynski et al. 2015b, 2016) over 45 500 RR Lyrae stars and 9500 Cepheids in the Magellanic Clouds. *Gaia* will revise upwards these statistics as ongoing surveys such as OGLE-IV (Soszynski et al. 2015a,b,c, 2016), Catalina Sky Survey (CSS, Drake et al. 2013; Torrealba et al. 2015), Pan-STARRS (Hernitschek et al. 2016), LINEAR (Sesar et al. 2013), and PTF (Cohen et al. 2016) are constantly reporting new discoveries and increased numbers of RR Lyrae stars and Cepheids both in the MW and in its neighbour companions.

Gaia's complete census of the Galactic Cepheids and RR Lyrae stars will allow a breakthrough in our understanding of the MW structure by tracing young and old variable stars all the way through from the Galactic bulge, to the disk, to the halo, and will likely reveal new streams and faint satellites that bear witness to the MW hierarchical build-up (see e.g. Clementini 2016). But most importantly, *Gaia* will measure the parallax of tens of thousands of Galactic Cepheids and RR Lyrae stars, along with milli-mag optical spectrophotometry (G broad-band white-light magnitude, blue and red spectro-photometry) and radial velocities and chemistry for those within reach of the Radial Velocity Spectrometer (RVS; $G \lesssim 17$ mag). The unprecedented accuracy of *Gaia* measurements for local Cepheids and RR Lyrae stars will allow the absolute calibration via parallax of the Cepheid *PL*, *PLC*, *PW* and of the M_V–[Fe/H] and infrared *PLZ* relations for RR Lyrae stars, along with a test of the metallicity effects through simultaneous abundance measurements. This will enable re-calibration of "secondary" distance indicators probing distances far into the unperturbed Hubble flow and a total re-assessment of the whole cosmic distance ladder, from local to cosmological distances, in turn significantly improving our knowledge of the Hubble constant. The physical parameters of Cepheids and RR Lyrae stars will be constrained by *Gaia* photometry, parallax, metallicity, and radial velocity (RV) measurements, which will in turn constrain the input physics of theoretical pulsation models. This will further improve the use of Cepheids and RR Lyrae stars as standard candles and stellar population tracers.

In this paper we describe the Specific Objects Study (SOS) pipeline developed within the Coordination Unit 7 (CU7) of the Data Processing and Analysis Consortium (DPAC), the coordination unit in charge of the processing and analysis of variable sources observed by *Gaia*, to validate and fully characterise Cepheids and RR Lyrae stars observed by the spacecraft. A detailed description of the *Gaia* mission, its scientific goals and performance, as well as a comprehensive illustration of the *Gaia* DPAC structure and activities can be found in Gaia Collaboration (2016c). A summary of the astrometric, photometric, and survey properties of *Gaia* Data Release 1 (*Gaia* DR1) and a description of scientific quality and limitations of this first data release are provided in Gaia Collaboration (2016a). The photometric dataset and the processing of the G-band photometry released in *Gaia* DR1 are thoroughly discussed in van Leeuwen et al. (2016), Carrasco et al. (2016), Riello et al. (in prep.), and Evans et al. (2016).

We note that a rather strict policy has been adopted within DPAC for the processing and dissemination of *Gaia* data. Specifically, it was decided to be consistent in how DPAC does the processing and what is published in *Gaia* releases. That is, we do not release results which are based on *Gaia* data that is not published. For instance, since no G_{BP}, G_{RP} photometry is released in *Gaia* DR1, only the G-band time series photometry was used for processing and classification of the variable sources released in *Gaia* DR1. Furthermore, characterisation and classification of *Gaia* variable sources rely only on *Gaia* data. That is, we do not complement *Gaia*'s time series with external non-*Gaia* data to increase the number of data points or the time-span of the *Gaia* observations. Literature published data are used once the processing is completed, but only to validate results (i.e. characterisation and classification of the variable sources), which are, however, purely and exclusively based on *Gaia* data. Whether – and how – this may have limited the efficiency of the *Gaia* pipeline for Cepheids and RR Lyrae stars is extensively discussed in the paper, most specifically in Sect. 3.2. On the other hand, we are also sure that the next *Gaia* data releases will significantly improve both census and results for variable stars, and will also emend misclassifications if and where they have occurred.

The SOS pipeline for Cepheids and RR Lyrae stars, hereafter referred to as SOS Cep&RRL pipeline, is one of the latest stages of the general variable star analysis pipeline. Steps of the processing prior the SOS Cep&RRL pipeline are fully described in Eyer et al. (2016), to which the reader is referred to for details.

Validation of the classification provided by the general variable star analysis pipeline is necessary, since Cepheids and RR Lyrae stars overlap in period with other types of variables (binary systems, long period variables, etc.). SOS Cep&RRL uses specific features such as the parameters of the light curve Fourier decomposition and diagnostic tools like the *Gaia* colour–magnitude diagram (CMD), the amplitude ratios, the period-amplitude (*PA*), *PL*, *PLC*, and *PW* relations, and the Petersen diagram (Petersen 1973) to check the classification, to derive periods and pulsation modes, and to identify multi-mode pulsators. Radial velocity measurements obtained by the RVS are also planned for use to identify binary/multiple systems as soon as they become available.

The main tasks of the SOS Cep&RRL pipeline are i) to validate and refine the detection and classification of Cepheids and RR Lyrae stars in the *Gaia* data base, provided by the general variable star analysis pipeline, by cleaning the sample from contaminating objects, i.e. other types of variables falling into

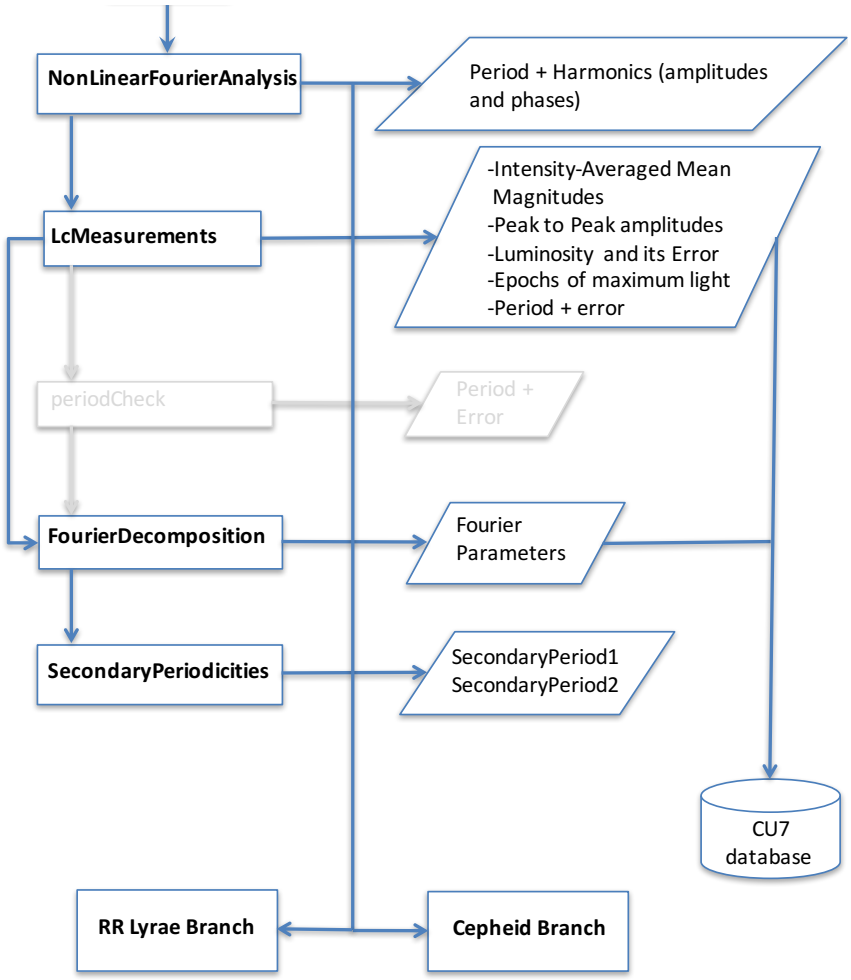

Fig. 1. Flow chart of the SOS Cep&RRL pipeline that is common to both Cepheid and RR Lyrae star processing. Boxes on the *left-hand* side show different modules of this general trunk, their outputs are indicated within rhombs on the *right-hand* side. Blue arrows connect modules activated for the processing of *Gaia* DR1 data, their names are highlighted in bold-face. We have marked in light grey modules not operational for the *Gaia* DR1 processing and their connections to the rest of the pipeline.

the same period domain; ii) to check and improve the period determination and the light curve modelling; iii) to identify the pulsation modes and the objects with secondary and multiple periodicities; iv) to classify RR Lyrae stars and Cepheids into subtypes (fundamental mode RRab, first overtone RRc, and double-mode RRd) according to the pulsation mode for the RR Lyrae stars, and DCEPs, ACEPs, and T2CEPs for the Cepheids, along with identification of pulsation modes for the first two, and subclassification into W Virginis (WVIR), BL Herculis (BLHER), and RV Tauri (RVTAU) types for the last; v) to identify and flag variables showing modulations of the light curve that are due to a binary companion or to the Blazhko effect (Blazhko 1907) that may falsify both the star brightness and the derived trigonometric parallax; vi) to use the pulsation properties and derive physical parameters (luminosity, mass, radius, effective temperature, metallicity, reddening, etc.) of confirmed bona fide RR Lyrae stars and Cepheids to be ingested into the *Gaia* main database by means of a variety of methods specifically tailored to these types of variables.

The paper is organised as follows. Section 2 provides a description of the whole architecture of the SOS Cep&RRL pipeline, its diagnostic tools, and their definition in the *Gaia* passbands. Sect. 3 presents the dataset and source selection on which the SOS Cep&RRL pipeline was run and describes how the pipeline was specifically tailored and simplified to analyse the *Gaia* SEP *G*-band time series data of candidate Cepheids and RR Lyrae stars. Section 4 presents the results of the SOS Cep&RRL analysis that are published in *Gaia* DR1. Finally, the main results and future developments of the pipeline are summarised in Sect. 5.

2. SOS Cep&RRL pipeline

In this section we present the SOS Cep&RRL pipeline in its complete form, briefly describing all its algorithms and tools, only part of which could actually be applied due to the specific characteristics of the dataset published in *Gaia* DR1 (see Sect. 3.2 for details).

In order to validate and refine the classification of Cepheids and RR Lyrae stars provided by the general variable star analysis pipeline, and be able in the future to make comparisons with the parameters measured for these stars by other DPAC processing tasks, different procedures are implemented in the SOS Cep&RRL pipeline as described in the following sections. The whole processing of the SOS Cep&RRL pipeline is presented schematically in Figs. 1–3 and described in detail in Sects. 2.1, 2.3 and 2.4. For each candidate confirmed as a bona fide RR Lyrae star or Cepheid, SOS Cep&RRL returns the most

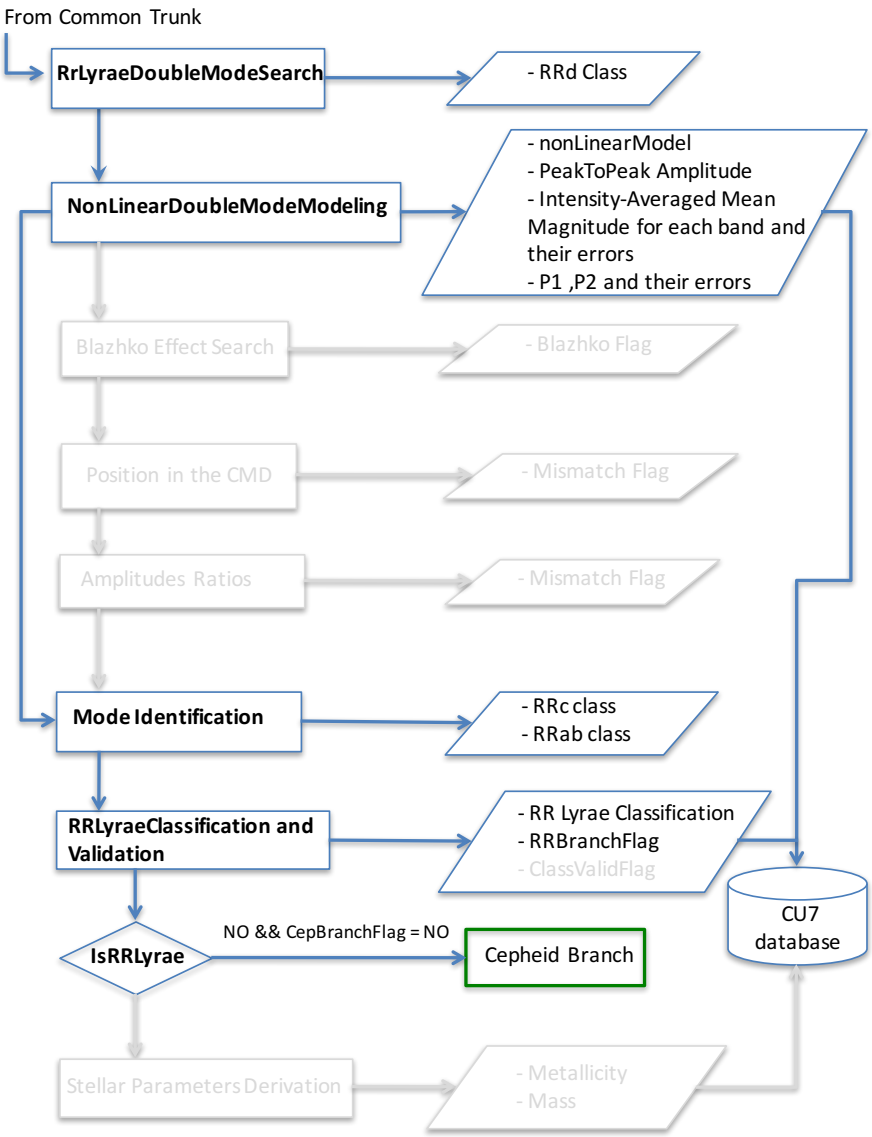

Fig. 2. Flow chart of the RR Lyrae branch in the SOS Cep&RRL pipeline. Boxes on the *left-hand* side show the different modules and their outputs are indicated within rhombi on the *right-hand side*. Blue arrows connect modules activated for the processing of the *Gaia* DR1 data; their names are highlighted in bold-face. We have marked in light grey modules not operational for the *Gaia* DR1 processing, their outputs, and their connections to the rest of the pipeline.

probable period, pulsation mode, multiple periodicities, if any, associated amplitudes, intensity-averaged magnitudes and mean radial velocities (if RVS data are available) as well as flagging of binary or multiple systems, to be published in the *Gaia* main data base.

The main input of SOS Cep&RRL is the calibrated *Gaia* time series photometry (*G*-magnitudes and integrated $G_{\rm BP}$, $G_{\rm RP}$ photometry) processed by CU5, the DPAC coordination unit charged with the photometric processing of *Gaia* data, for all sources pre-classified as candidate Cepheids and RR Lyrae stars by the general variability *Characterization* and *Classification* processing, along with general information on the data, such as number of transits per source (after outlier removal), typical errors, time span of the observations, mean and median magnitude values, etc., computed by the *Statistical Parameters* module in the general pipeline (Eyer et al. 2016) prior SOS Cep&RRL.

Additional information will be progressively added in future releases: RV time series for sources within the RVS magnitude limit, *Gaia*'s parallaxes (distances), and astrophysical parameters such as effective temperature ($\log T_{\rm eff}$), gravity ($\log g$), and absorption (A_λ) inferred by combining *Gaia*'s astrometry, photometry, and spectroscopy. This information can be used to optimise the SOS Cep&RRL processing.

2.1. Initial processing: characterisation of the light curves (period search and Fourier fitting)

The SOS Cep&RRL processing starts by characterising the *G*-band light curve (as well as the $G_{\rm BP}$ and $G_{\rm RP}$ light curves and the RVS RV curve if/when available) of sources classified as candidate Cepheids and RR Lyrae stars by the *Supervised Classification* module of the general variable star analysis pipeline. This part of the SOS Cep&RRL processing is common to both Cepheids and RR Lyrae stars and its main steps are shown in Fig. 1. The first step is the derivation of the source periodicity independently and with a different method to that used in the general pipeline *Characterization* module. We used the Lomb-Scargle algorithm (Lomb 1976; Scargle 1982)

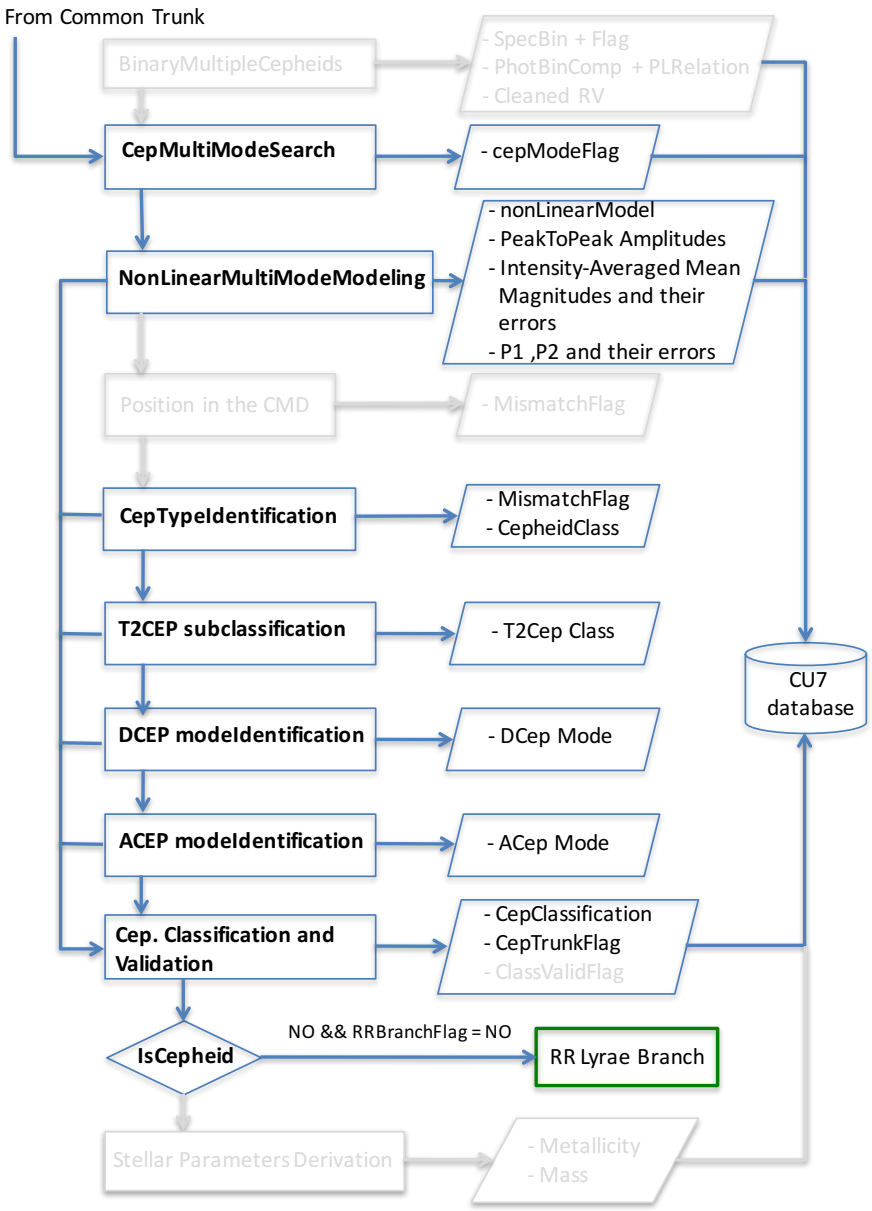

Fig. 3. Flow chart of the Cepheid branch in the SOS Cep&RRL pipeline. Layout and colour-coding are the same as in Fig. 2.

as opposed to the least-squares method used in *Characterization* (see Eyer et al. 2016). Tests performed on Cepheids and RR Lyrae stars in the HIPPARCOS catalogue showed that the Lomb-Scargle method reduces the number of large deviating period values for these specific types of variables. The period derived by SOS Cep&RRL is used to fold the light curve, which is then modelled with a truncated Fourier series in the form:

$$\mathrm{mag}(t_j) = zp + \sum [A_i \sin(i \times 2\pi\nu_{\max} t_j + \phi_i)]. \quad (1)$$

Zero-point (zp), period ($1/\nu_{\max}$), harmonic number (i), amplitudes (A_i), and phases (ϕ_i) of the harmonics for the G-band light curve are first computed with a linear fitting procedure. They provide initial trial values for the non-linear modelling of the light curve which is performed using the Levenberg-Marquardt (Levenberg 1944; Marquardt 1963) non-linear fitting algorithm (module *NonLinearFourierAnalysis* in Fig. 1). The non-linear fitting refines both the period and model of the light curve. In *Gaia* DR1 only the G-band time series photometry is available for the sources, hence the period resulting from the non-linear fitting of the G-band light curve is the final period adopted for the source, and module *LcMeasurements* directly measures the source intensity-averaged G mean magnitude, peak-to-peak G-amplitude, and epoch of maximum light from the G-band light curve modelled with the non-linear fitting algorithm[1]. The peak-to-peak G-amplitude [Amp(G)] is calculated as the (maximum) − (minimum) values of the model which fits the folded light curve best. An estimate of the error on this quantity is provided by $\sqrt{2}\times\sigma(zp)$. The epoch of maximum light is computed as the Baricentric Julian day (BJD) of the maximum value of the G-band light curve model which is closer to

[1] An independent search for the best period and best-fit model calculations will be performed on the $G_{\rm BP}$, $G_{\rm RP}$, and RV data when they become available. Peak-to-peak amplitudes and amplitude ratios for all photometric bands will be computed and an internal consistency check among periods from different passbands will be performed by the *periodCheck* module (see Fig. 1). This module was not activated for DR1.

the BJD of the first observations minus 3 times the period of the source. This procedure ensures that the time of maximum light precedes the time of the first observation. The mentioned BJD is offset by JD 2 455 197.5 d (= J2010.0). Adopting the results of the non-linear modelling amplitude ratios ($R_{ij} = A_i/A_j$), the phase differences ($\phi_{ij} = j \times \phi_i - i \times \phi_j$) and related errors of the Fourier decomposition of the G-band light curve are computed by the module *FourierDecomposition*[2]. Errors for all the parameters (period, amplitude, zp, etc.) derived with the non-linear Fourier modelling are estimated via Monte Carlo simulations[3] according to the following procedure:

- a new light curve is generated where (value of each phase point) = (value of the original phase point) + (random number) × (±error of the original phase point value). Random numbers range between 0 and 1;
- a new model is computed with the non-linear modelling procedure, using as trial values the model parameters of the original light curve;
- the first two steps are iterated 100 times;
- for each parameter of the model, average and standard deviation are computed over the 100 simulations;
- the standard deviations derived in the previous step are assigned as uncertainties of the parameters resulting from the non-linear modelling.

The final step in the general part of the SOS Cep&RRL pipeline is the detection of possible secondary periodicities in the source periodogram. This is the task of the *SecondaryPeriodicities* module. For RR Lyrae stars we look for one additional frequency and for Cepheids for two beyond the first periodicity. Following the procedure adopted in the *NonLinearFourierAnalysis* module, the residuals (observed − model phase points) are searched for secondary periodicities. If a significant secondary frequency is found the procedure is iterated twice. The steps of the *SecondaryPeriodicities* algorithm are as follows:

1. residuals are computed as (observed) − (corresponding model) phase points;
2. the Lomb-Scargle period search method is run on the residual time series.

This module will be revised in preparation for the *Gaia* second data release (*Gaia* DR2) in order to properly take into account the actual significance of the detected secondary periodicities (see Sect. 5).

After this common part the analysis proceeds in two separate branches each specifically tailored to the processing of RR Lyrae stars and Cepheids. This is summarised in the flow charts in Figs. 2 and 3. Sources classified as candidate Cepheids by the general *Classification* pipeline will be sent first to the Cepheid branch. Conversely, sources classified as candidate RR Lyrae stars will first be processed through the RR Lyrae branch. However, for the processing of the *Gaia* DR1 data we followed a different approach to decide which branch a source should be sent to (see Sect. 3.2).

2.2. Conversions to the Gaia passbands

A number of tools specifically applicable for the characterisation of RR Lyrae stars and Cepheids are adopted in the different modules of the Cepheid and RR Lyrae branches (see Figs. 2 and 3). They include the CMD; the G-band *PA* diagram (for RR Lyrae stars also known as the Bailey diagram; Bailey 1902); the *PL*, *PLC*, and *PW* relations for Cepheids; the different planes in the Fourier parameter space; and the Petersen diagram (Petersen 1973) for double-mode Cepheids and RR Lyrae stars. All limits and loci of these tools are defined for the Johnson photometric system. We have converted them to the *Gaia* photometric system in order to apply them directly to *Gaia* sources. We have used the passband transformations provided in Jordi et al. (2010) and subsequent updates (Jordi, priv. comm.) to compute conversion formulae appropriate for the colour and metallicity ranges of Cepheids and RR Lyrae stars ($V - I < 2.5$ mag and $-2.5 <$ [Fe/H] < 0.5 dex) and to transform the Johnson-Cousins V, I to the *Gaia* G, $G_{\rm BP}$, $G_{\rm RP}$ passbands. The conversion formula for the G band is provided in Appendix A and shown in Fig. A.1. We then used a sample of 128 RR Lyrae stars belonging to the Galactic halo and bulge, to the Galactic globular clusters M 3 and M 68, and to the Large Magellanic Cloud (LMC) and Small Magellanic Cloud (SMC) and also 77 classical Cepheids in the MW, LMC, and SMC, for which excellent light curves in the Johnson V and I passbands have been published by Soszynski et al. (2008a, 2009, 2010a,c, 2011a), Cacciari et al. (2005), Walker (1994), Moffett & Barnes (1984), Gieren (1981), Coulson & Caldwell (1985), Coulson et al. (1985), and Berdnikov & Turner (1995), Berdnikov et al. (2012, 2014). The two samples cover entirely the parameter space of pulsation modes, periods and metallicities for RR Lyrae stars and Cepheids. We used Eq. (A.1) to transform the V, I light curves of these selected samples to the *Gaia* G passband and fitted both original V, I, and *Gaia*-transformed G-band light curves with truncated Fourier series obtaining R_{21}, R_{31}, ϕ_{21}, ϕ_{31} parameters and peak-to-peak amplitude in each band. Finally, we used the quantities obtained with the above procedure to derive relationships and transform the Fourier parameters and peak-to-peak amplitudes from the Johnson-Cousins to the *Gaia* G band. The relations obtained with this procedure are described by Eqs. (2) to (19)[4].

Formulae to convert the literature peak-to-peak amplitudes of RR Lyrae stars to the *Gaia* G band are provided by Eqs. (2) and (3):

$$A(G) = (1.374 \pm 0.011) \times A(I) + (0.031 \pm 0.006) \quad \text{rms} = 0.025 \text{ mag} \tag{2}$$

$$A(G) = (0.925 \pm 0.003) \times A(V) - (0.012 \pm 0.003) \quad \text{rms} = 0.011 \text{ mag}. \tag{3}$$

We show in Fig. 4 the *PA* diagram in the *Gaia* G band of RR Lyrae stars in the LMC, the SMC, and the Galactic bulge and halo, obtained by converting the literature V and I amplitudes using Eqs. (2) and (3). We used literature amplitudes from Soszynski et al. (2009, 2010c, 2011a) for the RR Lyrae stars in the Magellanic Clouds, and from Pojmanski (1997) for the Galactic variables. In the figure a black solid line is drawn to separate RRab from RRc types. Also shown in the figure are ACEPs (filled circles) and T2CEPs (crosses) in the LMC and SMC taken from Soszynski et al. (2008b, 2015a). Their amplitudes were also transformed to the G band using Eqs. (2) and (3), since colours and amplitudes of ACEPs and T2CEPs are similar to those of RR Lyrae stars. The diagram in Fig. 4 is the main tool used to separate RR Lyrae stars into RRab and RRc types

[2] Fourier parameters will also be computed in the future for the $G_{\rm BP}$, $G_{\rm RP}$ light curves and for the RV curve to perform consistency checks.

[3] The only exceptions are the errors of the Fourier parameters ϕ_{ij} and R_{ij}, which are currently computed by propagation of the errors in ϕ_i, ϕ_j, R_i, and R_j, the last being computed via Monte Carlo simulations.

[4] The $G-I$ conversions are particularly valuable since the OGLE team usually publishes results for RR Lyrae stars and Cepheids in the I band.

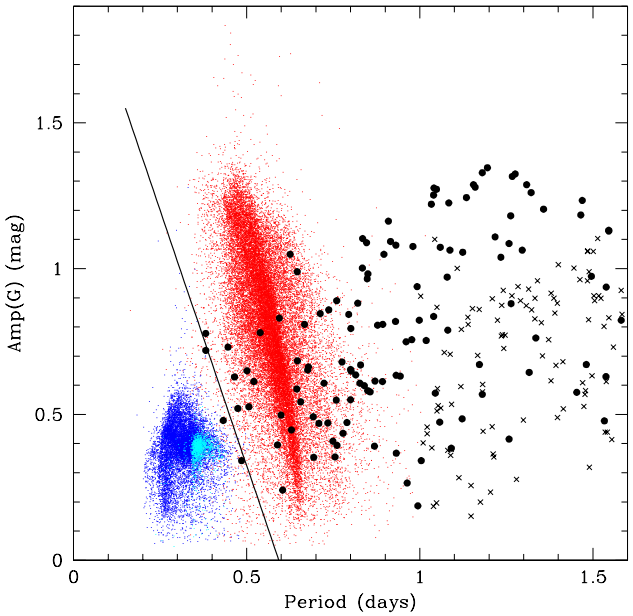

Fig. 4. *G*-band *PA* diagram for RR Lyrae stars (blue: RRc, cyan: RRd, red: RRab pulsators), ACEPs (black filled circles), and T2CEPs (crosses) obtained by converting to *G*-band literature photometry from the catalogues of RR Lyrae stars, ACEPs and T2CEPs of the OGLE, and ASAS surveys of the LMC, SMC, and Galactic bulge and halo, by Soszynski et al. (2008b, 2009, 2010b,c, 2011a,b), Poleski et al. (2010), and Pojmanski (1997). The black solid line separates RRc from RRab types. Contamination between the two pulsation modes occurs close to the separation line; further contamination is also due to ACEPs.

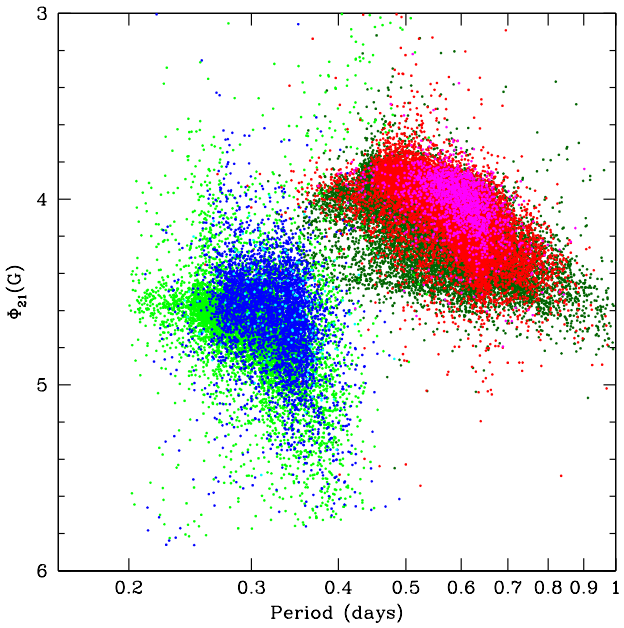

Fig. 5. *G*-band ϕ_{21} vs. period diagram for RR Lyrae stars in the LMC (red: RRab, blue: RRc), SMC (magenta: RRab, cyan: RRc), and Galactic bulge (dark green: RRab, green: RRc) obtained by converting the literature *I*-band ϕ_{21} values from OGLE to *G* band (see text for details).

(see Sect. 3). However, since mixing of the pulsation modes occurs close to the separation line and further contamination is also caused by ACEPs, we also used the Fourier parameters to separate different pulsation modes and variable types.

Equations (4) to (11) provide formulae to convert the literature values of the Fourier parameters R_{21}, R_{31}, ϕ_{21}, and ϕ_{31} of RR Lyrae stars to the *Gaia G* band:

$$\phi_{21}(G) = (0.35 \pm 0.07) + (0.816 \pm 0.016) \times \phi_{21}(I) - (0.64 \pm 0.06) \times \log P(\mathrm{d}) \quad \mathrm{rms} = 0.06 \tag{4}$$

$$\phi_{21}(G) = (0.13 \pm 0.03) + (0.996 \pm 0.007) \times \phi_{21}(V) + (0.22 \pm 0.03) \times \log P(\mathrm{d}) \quad \mathrm{rms} = 0.26 \tag{5}$$

$$\phi_{31}(G) = (-0.50 \pm 0.05) + (0.875 \pm 0.018) \times \phi_{31}(I) - (1.10 \pm 0.11) \times \log P(\mathrm{d}) \quad \mathrm{rms} = 0.11 \tag{6}$$

$$\phi_{31}(G) = (0.104 \pm 0.020) + (1.000 \pm 0.008) \times \phi_{31}(V) \quad \mathrm{rms} = 0.055 \tag{7}$$

$$R_{21}(G) = (0.029 \pm 0.005) + (0.953 \pm 0.011) \times R_{21}(I) - (0.05 \pm 0.02) \times \log P(\mathrm{d}) \quad \mathrm{rms} = 0.017 \tag{8}$$

$$R_{21}(G) = (0.000 \pm 0.002) + (1.015 \pm 0.004) \times R_{21}(V) \quad \mathrm{rms} = 0.006 \tag{9}$$

$$R_{31}(G) = (0.034 \pm 0.004) + (0.935 \pm 0.011) \times R_{31}(I) - (0.07 \pm 0.02) \times \log P(\mathrm{d}) \quad \mathrm{rms} = 0.015 \tag{10}$$

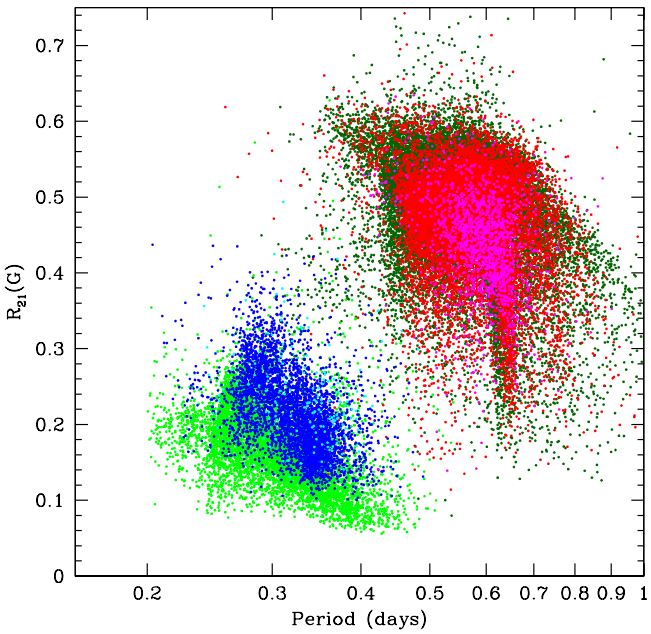

Fig. 6. Same as in Fig. 5, for the *G*-band R_{21} vs. period diagram.

$$R_{31}(G) = (-0.001 \pm 0.001) + (1.018 \pm 0.004) \times R_{31}(V) \quad \mathrm{rms} = 0.004. \tag{11}$$

Figures 5 and 6 show the *G*-band Fourier parameters ϕ_{21} and R_{21} of RR Lyrae stars computed using Eqs. (4), (5), (8), and (9) plotted versus period (P). The ϕ_{21} vs. P plot was used along with the *PA* diagram to distinguish RR Lyrae stars from ACEPs and to better separate the RRab and RRc types (see Sect. 3).

Finally, Eqs. (12) to (19) provide formulae to convert the literature values of the Fourier parameters R_{21}, R_{31}, ϕ_{21}, and ϕ_{31} of

Cepheids to the *Gaia G* band:

$$\phi_{21}(G) = (0.76 \pm 0.14) + (0.81 \pm 0.03) \times \phi_{21}(I) - (0.11 \pm 0.04) \times \log P(\mathrm{d}) \quad \mathrm{rms} = 0.088 \tag{12}$$

$$\phi_{21}(G) = (0.19 \pm 0.08) + (0.959 \pm 0.017) \times \phi_{21}(V) + (0.10 \pm 0.02) \times \log P(\mathrm{d}) \quad \mathrm{rms} = 0.063 \tag{13}$$

$$\phi_{31}(G) = (0.00 \pm 0.04) + (1.006 \pm 0.011) \times \phi_{31}(I) - (0.50 \pm 0.11) \times \log P(\mathrm{d}) \quad \mathrm{rms} = 0.095 \tag{14}$$

$$\phi_{31}(G) = (0.061 \pm 0.018) + (0.980 \pm 0.006) \times \phi_{31}(V) \quad \mathrm{rms} = 0.053 \tag{15}$$

$$R_{21}(G) = (0.014 \pm 0.007) + (0.98 \pm 0.02) \times R_{21}(I) \quad \mathrm{rms} = 0.018 \tag{16}$$

$$R_{21}(G) = (0.002 \pm 0.004) + (0.996 \pm 0.012) \times R_{21}(V) \quad \mathrm{rms} = 0.01 \tag{17}$$

$$R_{31}(G) = (0.005 \pm 0.006) + (0.99 \pm 0.03) \times R_{31}(I) \quad \mathrm{rms} = 0.012 \tag{18}$$

$$R_{31}(G) = (0.003 \pm 0.003) + (1.002 \pm 0.017) \times R_{31}(V) \quad \mathrm{rms} = 0.005. \tag{19}$$

Figures 8 and 9 show the G-band Fourier parameters ϕ_{21} and R_{21} of Cepheids computed using Eqs. (12), (13), (16), and (17) plotted versus period. These diagrams were used to distinguish different Cepheid modes and to separate Cepheids from RR Lyrae stars (see Sect. 3).

2.3. RR Lyrae branch

The different steps of the processing for sources classified as RR Lyrae stars by the general *Classification* pipeline are summarised in Fig. 2. However, only some modules of the RR Lyrae branch were activated for the analysis of the *Gaia* DR1 data.

2.3.1. Identification of double-mode RR Lyrae stars: *RRLyraeDoubleModeSearch* module

For RR Lyrae stars for which a secondary periodicity was detected by the *SecondaryPeriodicities* module of the initial SOS Cep&RRL processing (see Fig. 1), the *RRLyraeDoubleModeSearch* module sets the shorter and the longer periodicities to first overtone period (P_{1O}) and fundamental mode period (P_F), respectively. Then if both P_{1O} and P_F are longer than 0.3 d, it checks whether the star locates within the regions of the P_{1O}/P_F vs. P_F plane (generally known as the Petersen diagram; Petersen 1973) allowed for RR Lyrae double-mode pulsation. The allowed loci in the Petersen diagram were defined using

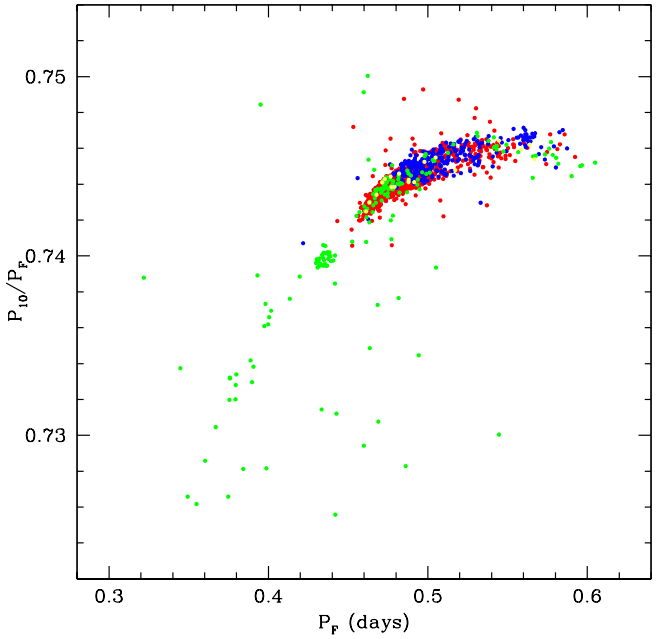

Fig. 7. Petersen diagram of double-mode RR Lyrae stars observed by the OGLE and ASAS surveys in the LMC (red filled circles), SMC (blue filled circles), and in the Galactic bulge (green filled circles) and halo (yellow filled circles). P_F and P_{1O} are the fundamental and first overtone pulsation mode, respectively (see text for details).

the P_{1O}, P_F, and P_{1O}/P_F values of 1335 RRd variables observed by the OGLE and ASAS surveys of the LMC, SMC, Galactic bulge, and halo. Their Petersen diagram is shown in Fig. 7. A lower limit of 0.3 d for the P_{1O}, P_F values was also inferred from Fig. 7, which shows that no RRd pulsators are known with $P_F < 0.3$ d. Schematically, the *RRLyraeDoubleModeSearch* algorithm performs the following steps:

- computing the P_{1O}/P_F ratio;
- if the source falls in the region defined as $0.724 < P_{1O}/P_F < 0.752$ and $0.30 < P_F < 0.62$ days, then the RR Lyrae star is identified as RRd.

The light curve modelling of a confirmed double-mode RR Lyrae star is then refined in the *NonLinearDoubleModeModeling* module by applying the non-linear fitting procedure with the proper truncated Fourier series and simultaneously fitting the two pulsation modes. In a similar way, the period, the epoch, the peak-to-peak amplitudes, and the Fourier decomposition are recomputed and refined. The *RRLyraeDoubleModeSearch* module of SOS Cep&RRL was tested, but its results have not yet been included in *Gaia* DR1.

2.3.2. Blazhko effect search, position in the CMD, and amplitude ratios

There are three modules in the RR Lyrae branch (*BlazhkoEffectSearch*, *PositionInTheCMD*, and *AmplitudeRatios*) that could not be activated because in the *Gaia* DR1 we lack the information to properly operate them. They are briefly described in the following.

The *BlazhkoEffectSearch* module searches for RR Lyrae stars affected by the Blazhko effect (Blazhko 1907), a periodic modulation of the amplitude and/or the phase of the main pulsation that occurs on timescales typically varying from a few

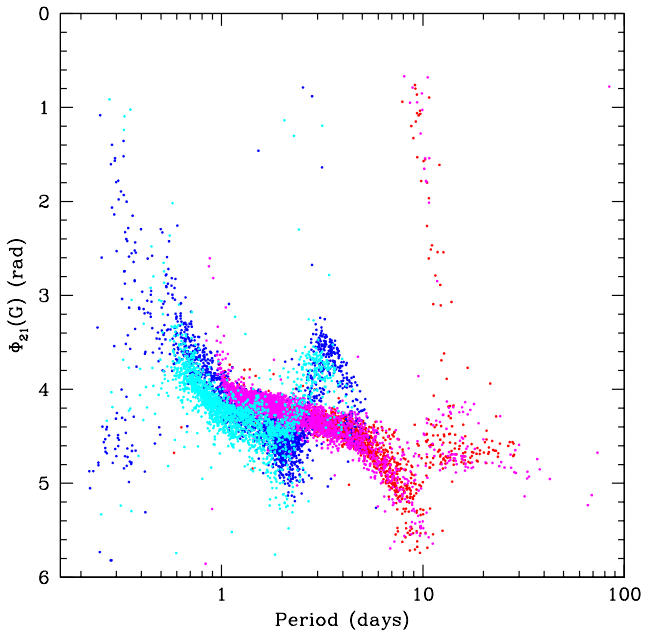

Fig. 8. *G*-band ϕ_{21} vs. period diagram for DCEPs in the Magellanic Clouds (red: F, blue: 1O DCEPs in the LMC; magenta: F, cyan: 1O DCEPs in the SMC). The figure was obtained by transforming the *I*-band ϕ_{21} values in Soszynski et al. (2008a, 2010a, 2015b,c) to the *G*-band using Eq. (12) (see text for details).

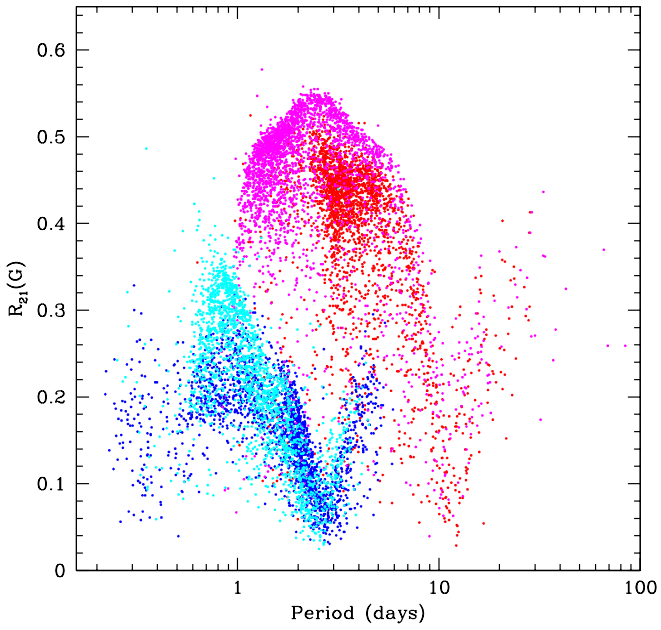

Fig. 9. *G*-band R_{21} vs. period diagram for DCEPs in the Magellanic Clouds (red: F, blue: 1O DCEPs in the LMC; magenta: F, cyan: 1O DCEPs in the SMC). The figure was obtained by transforming the *I*-band R_{21} values in Soszynski et al. (2008a, 2010a, 2015b,c) to the *G*-band using eq. (16) (see text for details).

days to hundreds of days. This phenomenon is shown by some 25−30% of the Galactic RRab and 5% of the RRc stars. However, recent detections of Blazhko stars with very small amplitudes suggest that these numbers may be underestimated (an occurrence rate as high as 50% follows from the studies by Jurcsik et al.; Jurcsik, priv. comm.). Using data from future releases, *Gaia* may provide accurate and updated occurrence rates. Radial velocity measurements and multi-band photometric data, to be obtained by *Gaia* with the foreseen long time base of observations, are fundamental to identify irregular and Blazhko variables among the RR Lyrae stars, and can help to understand whether they are due to non-radial modes excited during pulsation.

The *PositionInTheCMD* module verifies that sources classified as RR Lyrae stars fall inside the RR Lyrae instability strip (IS) in the CMD, by checking whether the colours of the targets are compatible with the IS for RR Lyrae stars. *Gaia* CMD is a fundamental tool used to clean the sample of RR Lyrae stars from possible contaminating objects, since other types of variables falling in the same period domain, for instance eclipsing binaries (ECLs), should lie predominantly outside the RR Lyrae IS in this diagram. Knowledge of the source absolute magnitude (via parallax) and colour (or effective temperature) are needed to use this tool. Parallaxes are published in *Gaia* in DR1 only for Cepheids and RR Lyrae stars with $G \lesssim 13.5$ mag as part of the Tycho-*Gaia* Astrometric Solution (TGAS; Lindegren et al. 2016). Cepheids and RR Lyrae stars for which results of the SOS Cep&RRL processing are published in *Gaia* DR1 are fainter than this limit (see Sect. 3.1), hence parallaxes are not yet available for them. This limited the use of the CMD tool (see Sect. 3).

The *AmplitudeRatios* module uses the peak-to-peak amplitude ratios between *Gaia*'s three different photometric bands to check whether the observed periodicity is due to a contact binary system mimicking an RR Lyrae-like light curve (this may be the case especially for RRc pulsators). In fact, amplitude ratios between different photometric bands are expected to be close to unity in the case of ECLs. Lacking G_{BP}, G_{RP} time series, this tool could not be activated for *Gaia* DR1.

2.3.3. PA diagram and mode identification: *ModeIdentification* module

RRab and RRc types occupy different locations in the *G*-band peak-to-peak amplitude vs. period diagram (see Fig. 4) and in the P–R_{21}, and P–ϕ_{21} planes (see Figs. 5 and 6). The *ModeIdentification* module combines results from these three diagnostics to identify the pulsation mode of candidate RR Lyrae stars and/or recognise misclassified objects. According to Fig. 4, RR Lyrae stars are confined within 0.2 d $\leq P \leq$ 1.0 d in period and within 0.05 mag $\leq$ Amp(G) $\leq$ 2.0 mag in *G*-band amplitude. Sources outside these ranges will be flagged as possible misclassified objects. Furthermore, RRc and RRab types can then be separated with a line described by the equation $\mathrm{Amp}(G) = -4.0 \times P + 2.2$. Mixing of RRc and RRab pulsators occurs close to the separation line, and significant contamination also exists in Fig. 4 between RR Lyrae stars and ACEPs. However, they can both be reduced by using the star position in the Fourier R_{21} and ϕ_{21} vs. P planes (Figs. 5 and 6) where the two types are located in separate regions whose borders we define in Sect. 4.

2.3.4. RR Lyrae star classification

This module performs the final assignment of a source to the RR Lyrae class based on results of the previous SOS Cep&RRL modules. If the source is confirmed to be an RR Lyrae star, thus validating the initial class assignment provided by the general *Classification* pipeline, the analysis proceeds with the

Table 1. Permitted periods and period ratios for multi-mode DCEPs.

0.7	$< P_{1O}/P_F <$ 0.76	&	$0.5 < P_F < 8$ d
0.79	$< P_{2O}/P_{1O} <$ 0.81	&	$0.15 < P_{1O} < 1.8$ d
0.67	$< P_{1O}/P_{3O} <$ 0.68	&	$0.5 < P_{1O} < 0.6$ d
0.58	$< P_{2O}/P_F <$ 0.68	&	$0.4 < P_F < 1.6$ d
0.655	$< P_{3O}/P_{1O} <$ 0.685	&	$0.1 < P_{1O} < 0.7$ d
0.828	$< P_{3O}/P_{2O} <$ 0.844	&	$0.15 < P_{2O} < 0.65$ d

derivation of the stellar parameters[5] and the final export of the source attributes (period, mean magnitude, peak-to-peak amplitude, Fourier parameters, secondary periodicity, pulsation mode, and any other relevant quantities) to the Main Data Base. Conversely, if the source is not confirmed as an RR Lyrae star, it is sent for analysis through the Cepheid branch (green box in Fig. 2) unless it was already analysed in that branch and not found to be a Cepheid either, in which case it will be definitively rejected as an RR Lyrae star and/or Cepheid and fed back to the general variable star analysis pipeline for processing through other SOS modules.

2.4. Cepheid branch

The processing of sources classified as Cepheid candidates by the general *Classification* pipeline occurs in the Cepheid branch first, the steps of which are schematically shown in Fig. 3. As with the RR Lyrae stars only some modules of the Cepheid branch could be used for the analysis of the Cepheids in *Gaia* DR1. In particular, the first step of the Cepheid branch processing would be the identification of Cepheids in binary or multiple systems using RV measurements obtained by the RVS and the ratios of photometric amplitudes in the different passband. Since neither RVs nor G_{BP}, G_{RP} photometry is available in *Gaia* DR1, this module was not activated. Similarly, we could not use the *PositionInTheCMD* module to check whether the candidate Cepheids fell inside the DCEP, ACEP, and TCEP instability strips in the CMD. Analysis in the Cepheids branch starts from the search for multi-mode variables performed by the *CepMultModeSearch* module.

2.4.1. Identification of multi-mode Cepheids: *CepMultiModeSearch* module

The *CepMultiModeSearch* module identifies Cepheids pulsating simultaneously in different modes by checking the period ratios of the different periodicities found by the *SecondaryPeriodicities* module of the general trunk (Fig. 1). The relevant period ratios are 1O over F (P_{1O}/P_F), second-overtone (2O) over F (P_{2O}/P_F), and so on (P_{2O}/P_{1O}; P_{3O}/P_{1O}; P_{3O}/P_{2O}). The typical values for these ratios are known both from empirical and theoretical studies. Allowed periods and period ratios for multi-mode DCEPs, following Soszynski et al. (2008a), are reported in Table 1.

The following different cases are considered, depending on the number of secondary periodicities found by the *SecondaryPeriodicities* module of the SOS Cep&RRL general trunk:

- *case 1: two periodicities are found*
  - The algorithm sets the shorter and the longer periodicities to P_{1O} and P_F, respectively. Then it checks whether the ratio P_{1O}/P_F falls within the allowed ranges listed in Table 1.
  - The algorithm sets the shorter and the longer periodicities to P_{2O} and P_F, respectively. Then it checks whether the ratio P_{2O}/P_F is within the allowed ranges, as listed in Table 1.
  - The algorithm sets the shorter and the longer periodicities to P_{2O} and P_{1O}, respectively. Then it checks whether the ratio P_{2O}/P_{1O} is within the allowed ranges, as listed in Table 1.
  - The algorithm sets the shorter and the longer periodicities to P_{3O} and P_{1O}, respectively. Then it checks whether the ratio P_{3O}/P_{1O} is within the allowed ranges, as listed in Table 1.

  If none of the above conditions is satisfied the source is rejected as a multi-mode Cepheid.
- *case 2: three periodicities are found*
  - The algorithm sets the shortest, the intermediate, and the longest periodicity to P_{2O}, P_{1O}, and P_F, respectively. Then it checks whether the P_{1O}/P_F, P_{2O}/P_F, and P_{2O}/P_{1O} ratios are within the allowed ranges, as listed in Table 1.
  - The algorithm sets the shortest, the intermediate, and the longest periodicity to P_{3O}, P_{2O}, and P_{1O}, respectively. Then it checks whether the P_{3O}/P_{1O}, P_{3O}/P_{2O}, and P_{2O}/P_{1O} ratios are within the allowed ranges, as listed in Table 1.

  If none of the above conditions is satisfied the source is rejected as a multi-mode Cepheid.

The light curve modelling of a confirmed multi-mode Cepheid is refined in the *NonLinearDoubleModeModeling* module by applying the non-linear fitting procedure with the proper truncated Fourier series and fitting simultaneously all pulsation modes (generally two). Periodicities, epoch of maximum light, intensity-averaged mean magnitude, peak-to-peak amplitudes of the two/three pulsation modes, and the parameters of the Fourier decomposition are also recomputed and refined taking into account all periodicities. The *CepMultiModeSearch* module of SOS Cep&RRL was tested, but its results have not yet been included in *Gaia* DR1.

2.4.2. Identification of Cepheid type (DCEP, ACEP, T2CEP): *CepTypeIdentification* module

The *CepTypeIdentification* module combines pulsation and photometric characteristics (in the future also spectroscopic characteristics) of the candidate Cepheids computed in the previous modules of the SOS Cep&RRL processing (both in the general trunk and in the Cepheid branch) to subdivide them into DCEP, ACEP, and T2CEP types. The module foresees the use of two main diagnostics: (i) the source metallicity that will be derived by the DPAC processing of RVS measurements as DCEP and T2CEP/ACEP types in general show different metallicity

[5] This occurs through the *StellarParametersDerivation* module, which is still partially under development, where stellar intrinsic parameters are derived through a variety of methods specifically appropriate for RR Lyrae stars. These include radius estimates via Baade-Wesselink analysis (see e.g. Cacciari et al. 1989, 1992, and references therein); metallicity estimates from the ϕ_{31} parameter of the Fourier light curve decomposition; reddening estimates from the light and colour curves; and mass estimates for double-mode pulsators through the Petersen diagram and the pulsation equation (Di Criscienzo et al. 2004) for single-mode pulsators. No specific tool for detecting RR Lyrae stars in binary systems has been implemented in the pipeline yet as binary RR Lyrae stars are an extremely rare event; only one has been firmly established so far (Wade et al. 1999), less than two dozen candidates have been reported in total by Hajdu et al. (2015) and Liska et al. (2015), but none of them has been spectroscopically confirmed yet.

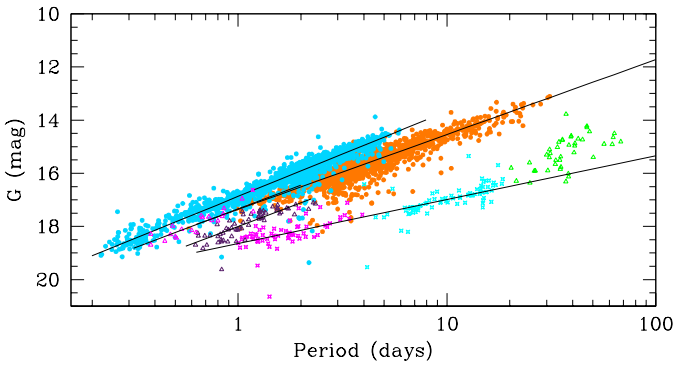

Fig. 10. *G*-band *PL* distribution of DCEPs, ACEPs, and T2CEPs in the LMC obtained transforming the OGLE *V, I* magnitudes to the *G*-band by means of Eq. (A.1). Overlaid are the *PL* relations described by Eqs. (20)−(24). Cyan filled circles: DECPs 1O; orange filled circles: DCEPs F; cyan four-starred symbols: ACEPs F; magenta four-starred symbols: ACEPs 1O; green open triangles: RVTAU; violet open triangles: WVIR; magenta open triangles: BLHER.

content, being the DCEPs typically more metal-rich than the T2CEPs and ACEPs, and (ii) the *PL* and *PW* relations, which are different for the three types of Cepheids. However, for *Gaia* DR1 the identification of the Cepheid types could rely only on the use of the *G*-band *PL* relations, for which we used the following set of equations

$$\mathrm{DCEP_F}: M_G = (17.361 \pm 0.020) - DM_{\mathrm{LMC}} - (2.818 \pm 0.032) \times \log P \quad \sigma = 0.162 \text{ mag} \tag{20}$$

$$\mathrm{DCEP_{1O}}: M_G = (16.872 \pm 0.010) - DM_{\mathrm{LMC}} - (3.195 \pm 0.030) \times \log P \quad \sigma = 0.181 \text{ mag} \tag{21}$$

$$\mathrm{T2CEP}: M_G = (18.640 \pm 0.085) - DM_{\mathrm{LMC}} - (1.650 \pm 0.109) \times \log P \quad \sigma = 0.188 \text{ mag} \tag{22}$$

$$\mathrm{ACEP_F}: M_G = (18.00 \pm 0.04) - DM_{\mathrm{LMC}} - (2.95 \pm 0.27) \log P \quad \sigma = 0.22 \text{ mag} \tag{23}$$

$$\mathrm{ACEP_{1O}}: M_G = (17.34 \pm 0.08) - DM_{\mathrm{LMC}} - (2.95 \pm 0.35) \times \log P \quad \sigma = 0.20 \text{ mag} \tag{24}$$

where M_G is the absolute magnitude in the G band. These relations were defined using Cepheids in the LMC for which light curves and pulsation characteristics have been published by Soszynski et al. (2008a,b), and adopting an absolute de-reddened distance modulus for the LMC of $DM_{\mathrm{LMC}} = 18.49$ mag from Pietrzynski et al. (2013). They are shown in Fig. 10. Candidate Cepheids that fall within 4σ of any of the above relations are assigned the Cepheid type and pulsation mode of the closest *PL*. Conversely, candidate Cepheids falling beyond 4σ will be rejected as misclassified sources. T2CEPs are further subdivided into three separate classes: the BLHER class, the WVIR class, and the RVTAU class, depending on the pulsation period. The three different subclasses of the T2CEP group follow different *PL* and *PW* relations and populate different period ranges. The *T2CEPSubclassification* module identifies the T2CEPs with periods in the range $1 \leq P < 4$ d as BLHER, the T2CEPs with periods in the range $4 \leq P < 20$ d as WVIR, and the T2CEPs with periods equal to or longer than 20 days as RVTAU (Soszynski et al. 2008b).

Single-mode DCEPs are known to pulsate in the F, 1O, and 2O modes. Since F, 1O, and 2O DCEP subclasses occupy different loci in the R_{21} vs. Period diagram, the *DCEPModeIdentification* module assigns the pulsation mode to a DCEP using the R_{21} parameter of the light curve Fourier decomposition. Specifically, considering the Fourier decomposition of the *G*-band light curve, and the R_{21} vs. P diagram, a DCEP will be pulsating in the 1O mode if the following conditions are verified,

$R_{21} < -0.13 \times P(\mathrm{d}) + 0.53$
and
$P < 2.34$ d or $R_{21} < 0.214$
and
$0.234 \text{ d} < P < 7$ d,

otherwise it is assigned the F mode. These limits were inferred from the *PL* relations of DCEPs based on OGLE-III data.

In Sect. 4 we discuss and illustrate graphically the regions we specifically defined in the ϕ_{21} and R_{21} vs. Period diagrams to separate Cepheids from RR Lyrae stars and to identify the Cepheid pulsation mode.

Similarly, ACEPs are known to pulsate in the F and 1O modes. The *ACEPModeIdentification* module assigns the pulsation mode to an ACEP by combining results from the classification in types based on the *PL* relations (*CepTypeIdentification* module) and the source period, as 1O ACEPs have periods in the range $0.35 < P \leq 1.20$ d, whereas F ACEPs have periods in the range $1.20 < P \leq 2.5$ d. These limits were inferred from *PL* relations of ACEPs based on OGLE-III data.

2.4.3. Cepheid classification

This module performs the final assignment of a source to the Cepheid class and its subclasses based on results of the previous SOS Cep&RRL modules. If the source is confirmed to be a Cepheid, thus validating the initial class assignment provided by the general *Classification* pipeline, the analysis proceeds with derivation of the stellar parameters[6] and the final export of the source attributes (period, mean magnitude, peak-to-peak amplitude, Fourier parameters, secondary periodicity, classification in Cepheid types, pulsation mode, and any other relevant quantities) to the Main Data Base. Conversely, if the source is not confirmed to be a Cepheid, it will be sent for analysis through the RR Lyrae branch (green box in Fig. 3), unless it was already analysed in that branch and not found to be an RR Lyrae star, in which case, it will be definitely rejected as a Cepheid and/or RR Lyrae star and fed back to the general variable star analysis pipeline for processing through other SOS modules.

[6] This occurs in the *StellarParametersDerivation* module. This module is under development and includes radius estimates via Baade-Wesselink analysis (see e.g. Barnes & Evans 1976; Ripepi et al. 1997); metallicity estimates for DCEPs from the R_{21} and R_{31} parameters of the Fourier light curve decomposition; identification of binary Cepheids from astrometry and RVS measurements and determination of their orbital elements; DCEP mass and age estimates.

3. Application of the SOS-Cep&RRL pipeline to *Gaia* DR1 dataset

Results on Cepheids and RR Lyrae stars published in *Gaia* DR1 are based only on the application of the SOS Cep&RRL pipeline to *Gaia* *G*-band time series photometry calibrated to the Vega magnitude system as no G_{BP}/G_{RP} photometry is published in the *Gaia* DR1, and parallax and RV information are not yet available for these Cepheids and RR Lyrae stars which are fainter than the TGAS sample (Lindegren et al. 2016). This made it necessary to rearrange and specifically tailor the SOS Cep&RRL pipeline to cope with the limited information available for the analysis of the Cepheid and RR Lyrae star candidates.

Processing of *Gaia* photometry takes place in an iterative manner organised through cycles (Evans et al. 2016). As detailed in Eyer et al. (2016), two datasets with different photometric calibration, time extent, and source number were used exceptionally in order to be able to publish Cepheids and RR Lyrae stars in advance of schedule for the *Gaia* DR1. The first dataset included Cycle 0 (C0) photometry of millions of objects observed in the first three months after commissioning (from July 25, 2014), which were reduced by the general variable star processing to a sample of under 20 K potential candidate Cepheids and RR Lyrae stars. This selection of sources was further analysed with the *Gaia* DR1 calibration photometry of Cycle 1 (C1), which spanned almost 14 months of observations.

The global variable star analysis performed for the *Gaia* first data release is schematically summarised in Fig. 11, which shows both the initial processing on the C0 dataset and the final processing of the C1 photometry released in *Gaia* DR1. The SOS Cep&RRL actual processing is detailed in Fig. 12 and specifically discussed in Sect. 3.2.

3.1. Dataset, source selection, and initial processing

The dataset processed by the SOS Cep&RRL pipeline to produce results published in *Gaia* DR1 consists of *G*-band time series photometry[7] of candidate Cepheids and RR Lyrae stars, observed by *Gaia* during 28-day ecliptic pole scanning law (EPSL) from the end of July to the end of August 2014, followed by over a year of nominal scanning law (NSL). We refer the reader to Sect. 5.2 in Gaia Collaboration (2016c) for a detailed description of *Gaia*'s scanning law. Source selection and steps of the preliminary analysis carried out on the C0 photometry (Evans et al. 2016) are summarised in the upper portion of Fig. 11. Sources were then reprocessed using the C1 photometry, producing the final results for Cepheids and RR Lyrae stars in the south ecliptic pole (SEP) footprint, which were published with the *Gaia* first data release. Only sources having 20 or more data points in the *G*-band time series were analysed as this was deemed to be the minimum number of epochs allowing a reliable estimate of the period and other (pulsation) characteristics of the confirmed variables. However, the actual number of epochs per source is <20 in some cases owing to the subsequent removal of outliers. As detailed in Eyer et al. (2016) and schematically summarised in Fig. 11, after applying the initial cut according to the number of epochs, the *Statistical Parameters* of the general variability pipeline computes the statistics of the time series data for all sources without any prior information on variability. Sources showing variability are then identified by the *General Variability Detection* module, characterised in terms of periodicity and

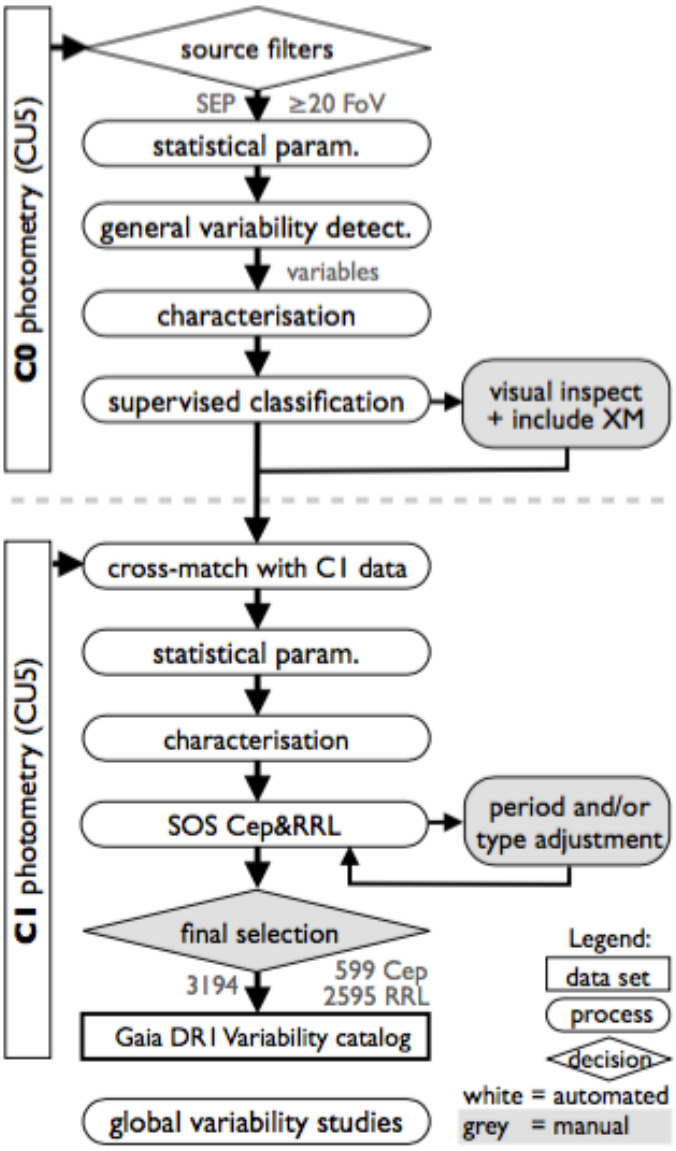

Fig. 11. Flow chart summarising the global variable star analysis pipeline adopted for *Gaia* first data release. See Fig. 10 in Eyer et al. (2016) for a more detailed version of this figure.

modelling of the light variation by the *Characterization* workpackage, and are finally sent to the *Supervised Classification* module to determine the variability type. The SOS Cep&RRL pipeline received sources classified as candidate Cepheids and RR Lyrae stars by the three classifiers (Gaussian Mixtures – GMs; Bayesian Networks – BNs, and Random Forests – RFs) operated by the *Supervised Classification* module of the general variable star analysis pipeline (see Eyer et al. 2016, and references therein for details). A sample of 19 923 source were initially classified as candidate RR Lyrae stars and Cepheids by applying the BN, RF, and GM classifiers to the C0 photometry of *Gaia* SEP region. Their distribution on sky is shown in Figs. 13 and 14. This rather large number of candidates included all probability levels and the candidates flagged as class outliers in order to maintain a high level of completeness and not lose potentially valid candidates.

The characteristic geometric shape of the area covered by *Gaia* SEP observations is mainly due to the way the spacecraft

[7] Each point in the *G*-band time series is the mean of the nine CCD measurements collected during one observation of a source by *Gaia*.

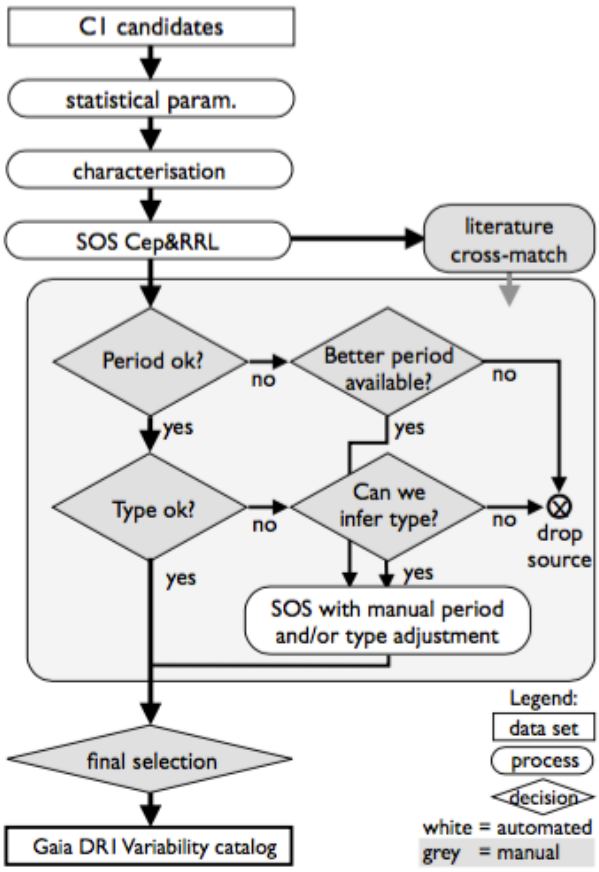

Fig. 12. Flow chart detailing the different steps of the SOS Cep&RRL pipeline actual processing applied to produce results for *Gaia* first data release.

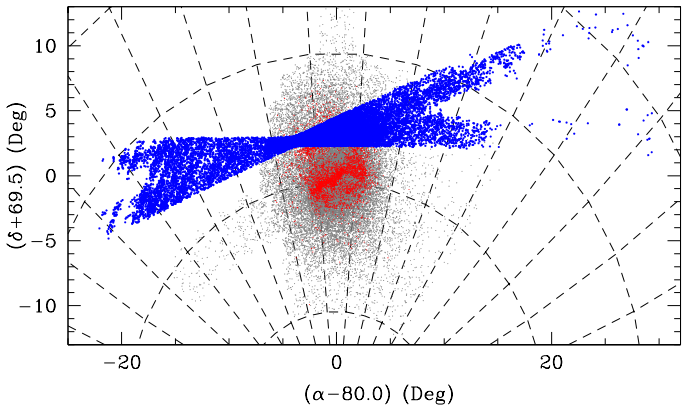

Fig. 13. Blue filled circles: distribution on sky of 19 923 sources in the *Gaia* SEP footprint, containing the enlarged set of Cepheid and RR Lyrae star candidates by the *Classification* workpackage of the general variable star analysis pipeline (9347 candidates + 10 576 candidate outliers). *Gaia* SEP intercepts an external region of the LMC. Grey and red filled circles are, respectively, RR Lyrae stars and Cepheids observed in the LMC by the OGLE survey (see text for details).

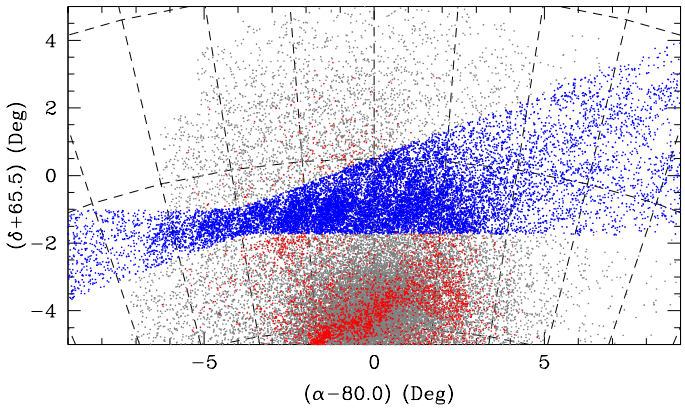

Fig. 14. Enlargement of Fig. 13 showing the region of the LMC covered by the *Gaia* SEP. Symbols and colour-coding are as in Fig. 13.

scanned the sky during the first 28 days of science operation in EPSL when *Gaia* was set to repeatedly monitor the two ecliptic poles. Therefore, sources very close (~1 deg) to the ecliptic poles may have time series data with more than 200 observations, though quickly dropping off at distances further away. *Gaia* SEP footprint intercepts a peripheral portion of the LMC, offset by about 3 degrees to the north and 4 degrees to the east of the LMC centre, which contains several Cepheids and RR Lyrae stars (as well as other types of variable stars) with characteristics known from the studies by the OGLE (Soszynski et al. 2012, 2015a,b,c, 2016, and references therein) and EROS-2 (according to Kim et al. 2014) surveys. They are shown as grey (RR Lyrae stars) and red (Cepheids) filled circles in Figs. 13 and 14.

Candidate Cepheids and RR Lyrae stars in the *Gaia* SEP most likely belong to the LMC, hence, to a first approximation, they are all the same distance from us. Due to the lack of parallaxes/distances to support the variability analysis of these sources at this early stage of the *Gaia* mission, this occurrence, along with the high cadence of the EPSL observations, were important assets that helped the SOS Cep& RRL processing for the first *Gaia* data release, which specifically focused on the 19 923 Cepheids and RR Lyrae star candidates within the *Gaia* SEP marked in blue in Figs. 13 and 14.

The scanning law determines the cadence of *Gaia* multi-epoch observations and, in turn, has a bearing on the alias patterns we may expect to show up in the power spectrum of *Gaia* time series data. Particularly strong is the 6 h alias caused by the spacecraft rotation around its axis, which during EPSL was always kept in the ecliptic plane and fixed with respect to the *Gaia*-Sun axis (see Sect. 3 in Eyer et al. 2016). This is clearly seen in the two panels of Fig. 15, which show the period – *G*-band amplitude distribution of the 19 923 candidate RR Lyrae stars and Cepheids in the *Gaia* SEP. Sources are plotted using the period computed by the *Characterization* workpackage of the general variability pipeline for Cepheid and RR Lyrae star candidates and OGLE's period for the known variables. The figure also shows that only very few of the known Cepheids and RR Lyrae stars in this region of the LMC have *G*-band amplitude smaller than 0.1 mag, hence suggesting that the vast majority of candidates with such small amplitudes are misclassifications, lending support to the choice of not considering them any further (see Sect. 3.2). Test runs of the SOS Cep&RRL pipeline along with visual inspection of a randomly selected sample of the 19 923 SEP Cepheid and RR Lyrae star candidates during this initial stage of the processing helped to provide a general overview of the dataset, improve the global analysis, and fine-tune the classifiers' predictions. The visual inspection also confirmed five candidates that were later added to the final counts.

By excluding sources flagged as RR Lyrae star and Cepheid outliers in the predictions of the used classifiers the sample of automatically identified Cepheid and RR Lyrae star candidates

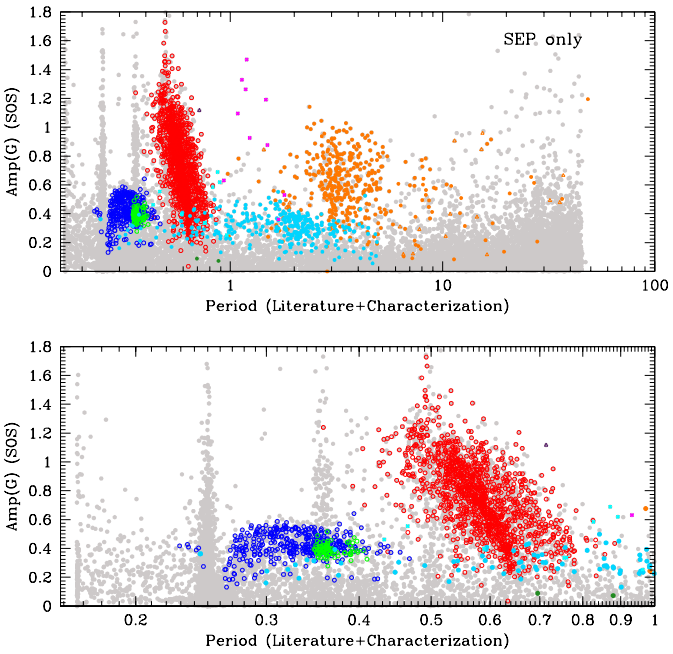

Fig. 15. P − G-band amplitude distribution of 19 923 candidate Cepheids and RR Lyrae stars (grey filled cicles) identified by the *Classification* pipeline of the general variability processing in the C0 photometry of the *Gaia* SEP. Units are in days and magnitude on the X- and Y-axis, respectively. The *bottom panel* is an expansion of the *top panel* for the region of $P \leq 1$ d. Orange and cyan filled circles mark F and 1O Cepheids; red, blue, and green open circles are RRab, RRc, and RRd pulsators known from the OGLE-III and OGLE-IV GSEP catalogues. Amplitudes are values computed by running the SOS Cep&RRL pipeline on C0 photometry. The strong peak around $P = 0.25$ d is an alias due to the rotation period of *Gaia* around its axis.

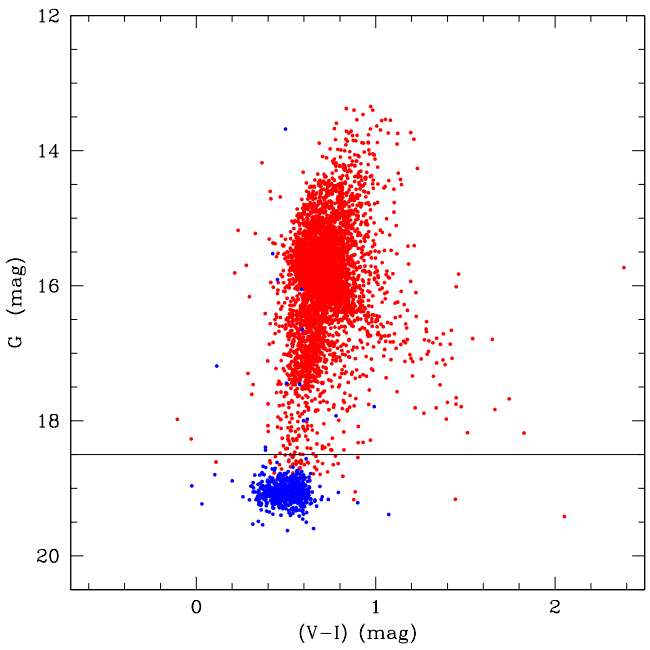

Fig. 16. G-band vs. $V - I$ colour−magnitude diagram of RR Lyrae stars (blue filled circles) and Cepheids (red filled circles) in the LMC field, using the OGLE-IV GSEP catalogue for the RR Lyrae stars (Soszynski et al. 2012) and OGLE-IV LMC Cepheids according to Soszynski et al. (2015a,b,c).

reduces to 9347 sources. Then, by further rejecting sources with G-band amplitudes smaller than 0.1 mag (more than 3800) but including the above-mentioned candidates identified by visual inspection, the number of SEP Cepheid and RR Lyrae star candidates drops to 6714 sources, 6053 of which were recovered by cross-matching the C0 and C1 photometries. This forms the sample finally processed through the SOS Cep&RRL pipeline.

Statistical properties (time sampling, number of observations, time series duration, mean/median G magnitudes, magnitude uncertainties, etc.) of the G-band C0 time series photometry out of which the initial 19 923 enlarged sample of Cepheid and RR Lyrae star candidates analysed by the SOS Cep&RRL pipeline was extracted are described in great detail in Sect. 5.2 and Figs. 14−17 of Eyer et al. (2016). Instead, the characteristics of the G-band C1 time series photometry of the sample of 6053 sources finally processed through the SOS Cep&RRL pipeline and turned into the 3194 confirmed Cepheids and RR Lyrae stars released in *Gaia* DR1 are described in Sect. 6.2, Figs. 27, 28, 30, 31 and Table 3 of Eyer et al. (2016).

We briefly note here that the latter sample spans the G-band magnitude range $12 \lesssim \langle G \rangle \lesssim 20.3$ mag with typical errors on the order of a few millimag and $\gtrsim$0.02 mag per individual data point at the bright and faint ends, respectively, G-band amplitudes in the range from ∼0.1 and 1.5 mag, and between 15 and over 200 phase-point sampling of the light curves (see text and figures in Sect. 4 for details).

Integrated blue (G_{BP}) and red (G_{RP}) spectrophotometry from the blue and red photometers on board *Gaia* was not released in *Gaia* DR1. This additional limitation of the *Gaia* DR1 dataset means we could not build the *Gaia* CMD of the SEP Cepheid and RR Lyrae star candidates. However, we built a G-band vs. $V - I$ CMD, shown in Fig. 16, using the OGLE-IV GSEP catalogue of LMC RR Lyrae stars (Soszynski et al. 2012) and the OGLE-IV catalogues of LMC Cepheids published by Soszynski et al. (2015b,c). The mean V magnitudes published by OGLE were transformed to the *Gaia* G-band using Eq. (A.1). This gave us some insight into the range in G magnitude spanned by RR Lyrae stars and Cepheids in the *Gaia* SEP (see Sect. 3.2).

The C1 time series photometry of the 6053 Cepheid and RR Lyrae star candidates, selected as described in Sect. 3.1, was fed into the SOS Cep&RRL pipeline. As a first step sources were cross-matched against catalogues of known RR Lyrae stars and Cepheids existing in the literature. We primarily used the OGLE-III (Soszynski et al. 2009) catalogue for RR Lyrae stars[8] OGLE-IV catalogue (Soszynski et al. 2015a,b,c) for Cepheids and the EROS-2 catalogue of Kim et al. (2014). We also used RR Lyrae stars and Cepheids identified in the SEP region by the Catalina (Torrealba et al. 2015,) and ASAS (Pojmanski 1997) surveys and also checked the online version of the GVCS[9] and the Simbad catalogue[10].

3.2. Tailoring the SOS Cep&RRL pipeline for the analysis of the SEP data

Given the limitations of the first *Gaia* data, the SOS Cep&RRL pipeline had to be properly tailored to successfully process

[8] The OGLE-IV catalogue of the LMC RR Lyrae stars (Soszynski et al. 2016) became available after the SOS Cep&RRL processing and was completed with the discovery of over 1000 new LMC RR Lyrae stars, 2/3 of which turned out to be in common with Soszynski et al. (2016).

[9] http://www.sai.msu.su/gcvs/gcvs/

[10] http://simbad.u-strasbg.fr/simbad/

the *Gaia* DR1 data. This occurred through the following assumptions and simplifications which had a significant impact on the pipeline effectiveness and enhanced the need for visual inspections and manual intervention to check and adjust results (see Fig. 12):

- Lacking parallaxes (distances) for the stars in the sample, we assumed that the SEP sources were all the same distance from us, which is an acceptable first approximation given that they are located primarily in the LMC, and we adopted a cut in apparent magnitude to initially separate Cepheids from RR Lyrae stars. A threshold was set using the CMD in Fig. 16 by which we assumed that candidates with $\langle G \rangle > 18.5$ mag are more likely RR Lyrae stars and after the general trunk (Fig. 1) they were sent to the RR Lyrae branch (Fig. 2) of the SOS Cep&RRL pipeline. Conversely, candidates with $\langle G \rangle < 18.5$ mag were sent to the Cepheid branch (Fig. 3). However, since the SEP sample might also include Galactic RR Lyrae stars projected against the LMC, candidates brighter than 18.5 mag, with $P < 1$ d, and G-band amplitudes larger than 0.5 mag were analysed in both Cepheid and RR Lyrae branches as the two types overlap in this region of the parameter space. A fine-tuning of the Fourier parameters and definition of strict loci in the ϕ_{21} vs. P and R_{21} vs. P planes (see Sect. 4) were adopted to distinguish bright MW RR Lyrae stars from Cepheids.

- Lacking source colours, the classification of Cepheids in different types and pulsation modes could only rely on the *PL* relations, complemented by visual inspection of the Fourier planes. Furthermore, without colours, the contaminations by ECLs (both for Cepheids and RRc) and by δ Scuti (particularly at the faint end of the LMC RR Lyrae star distribution, $\langle G \rangle \gtrsim 20.0$ mag) were issues that only a visual inspection of the light curves could resolve.

- The limited time span covered by the *Gaia* DR1 data, whose bulk spans roughly 28 d, made the measure of period most reliable only for Cepheids with periods shorter than about 10 d. In addition, the strong aliases affecting the SEP data required visual inspection of the light curves and manual intervention (period or type tagging of sources) to solve ambiguous cases.

When G_{BP}, G_{RP} colours, parallaxes, and an increasingly complete dataset becomes available in next *Gaia* releases, the need for visual inspection and manual intervention will definitely decrease.

For known Cepheids and RR Lyrae stars the periods measured by the SOS Cep&RRL pipeline (hereafter, P_{SOS}) were compared with the literature values. Agreement was deemed satisfactory if differences were within 0.01 d for the Cepheids and 0.001 d for RR Lyrae stars. When differences excede these limits, visual inspection of the light curve folded according to the two different periods helped to decide which periodicity to adopt[11]. Figure 17 shows the comparison with the literature of the periods finally adopted for the known RR Lyrae stars and Cepheids released in *Gaia* DR1. The flattening of RR Lyrae stars/Cepheids around $\Delta P = 0.001/0.01$ d occurs because we have assumed that P_{SOS} and the literature period are in agreement if they differ by less than 0.001 and 0.01 d for the RR Lyrae stars and Cepheids, respectively. A few sources above these limits in Fig. 17 are variables for which $\Delta P > 0.001/0.01$ d and P_{SOS} produce a better folding of the light curve than the literature period. Visual inspection of all light curves during final assessment of the SOS Cep&RRL results confirms that the comparison procedure described above worked well for the present dataset which does not contain many long period Cepheids (above 10 d).

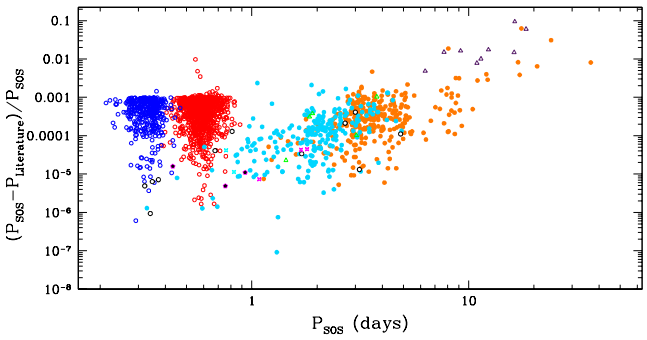

Fig. 17. Difference between the period computed by the SOS Cep&RRL pipeline (P_{SOS}) and the literature period for known RR Lyrae stars and Cepheids in the SEP region plotted vs. P_{SOS}. Blue open circles: RRc; red open circles: RRab; cyan filled circles: DECPs 1O; orange filled circles: DCEPs F; cyan four-starred symbols: ACEPs F; magenta four-starred symbols: ACEPs 1O; magenta pentagons filled in black: ACEPs without mode identification; green open triangles: BLHER; violet open triangles: WVIR; magenta open triangles: RVTAU; black open circles: DCEPs; and T2CEPs without mode or subtype identification.

Type and mode classification of the known RR Lyrae stars and Cepheids assigned by the SOS Cep&RRL pipeline were also cross-checked against literature. A number of obvious type misclassifications were emended by manual adjustment.

After processing through the SOS Cep&RRL pipeline the light curves of all 6063 candidates were visually inspected for data quality assurance, validation of the modelled light curve and quantities thereby derived (period, peak-to-peak amplitude, mean magnitude, etc.), and final assessment of the Cepheids and RR Lyrae stars to be published in *Gaia* DR1.

The run of the SOS Cep&RRL pipeline on the 6053 candidates combined with visual inspection of the resulting light curves produced a final sample of 3602 confirmed Cepheids and RR Lyrae stars and the rejection of a total number of 2451 sources. There are various reasons for this high number of rejections, including candidates identified in C0 which are not present in C1 photometry and photometry issues in the time series data among which very large outliers and/or systematically noisy light curves. However, the most important reason for rejection was incomplete sampling of the light curves resulting in unreliable values for the source period, peak-to-peak amplitude, and mean magnitude. Finally, further rejections were also due to contamination of the sample by ECLs and other types of variables (δ Scuti, LPVs, etc.). We explicitly note that a large fraction of these rejections (over 50%) are in fact bona fide RR Lyrae stars and Cepheids for which unambiguous determinations of period and/or type classification could be obtained, or are RR Lyrae stars and Cepheids that did not pass the strict quality control criteria we have adopted to validate these first variability results from *Gaia*. During quality assessment, it was also decided not to release results for double- or multi-mode sources (239 in total between RR Lyrae stars and Cepheids) as they were not fully compliant with our internal validation criteria. These criteria are quite strict to ensure a high reliability of the information

[11] For new RR Lyrae stars and Cepheids discovered by *Gaia*, such a check was performed by comparing P_{SOS} and the period computed by *Characterization* in the general variable star analysis pipeline.

Table 2. Number and type/mode classification of RR Lyrae stars and Cepheids published in *Gaia* DR1.

Type	total	New	Known
RRab	1910	228	1682
RRc	685	115	570
RR Lyrae total	2595	343	2252
DCEP F	313	12	301
DCEP 1O	230	10	220
DCEP NoMode[a]	15	4	11
DCEP total	558	26	532
ACEP F	6	3	3
ACEP 1O	7	5	2
ACEP NoMode[a]	3	0	3
ACEP total	16	8	8
T2CEP BLHER	11	6	5
T2CEP WVIR	10	1	9
T2CEP RVTAU	2	2	0
T2CEP NoSubType[a]	2	0	2
T2CEP total	25	9	16
Cepheid total	599	43	556

Notes. [(a)] With the terms NoMode and NoSubType, we have flagged sources for which the pulsation mode (for DCEPs and ACEPS) or the subtype (for T2CEP) could not be automatically and univocally identified by the SOS Cep&RRL pipeline.

for variable sources released in *Gaia* DR1, notwithstanding the actual limitations of the available dataset. By rejecting double-mode RR Lyrae stars and multi-mode Cepheids the sample was reduced to 3363 sources. Finally, 169 additional sources were rejected during the final validation process which was meant to achieve consistency on the total number of sources released by different tasks of the DPAC processing contributing results for *Gaia* DR1. This further trimming lead to a final sample of 3194 Cepheids and RR Lyrae stars.

4. Results

Position, G-band time series photometry, and final results of the SOS Cep&RRL pipeline were published in *Gaia* DR1 for a total of 3194 sources. They comprise 599 Cepheids (of which 43 are new from *Gaia*) and 2595 RR Lyrae stars (of which 343 are new discoveries). The subdivision of the 3194 sources according to type, subtype, and pulsation mode is summarised in Table 2.
For these 3194 sources the following parameters, computed by the SOS Cep&RRL pipeline, have been released in *Gaia* DR1 along with the related errors:

– source pulsation period;
– intensity-averaged mean G magnitude;
– epoch of maximum light;
– ϕ_{21} and R_{21} Fourier parameters;
– peak-to-peak G-band amplitude [Amp(G)];
– RR Lyrae star subclassification into RRab and RRc types;
– Cepheid classification into DCEP, ACEP, T2CEP types;
– DCEPs and ACEPs pulsation mode (F, 1O);
– T2CEPs subclassification into BLHER, WVIR, RVTAU types.

Gaia's sourceids, coordinates, values of the above quantities and associated statistics, along with the G-band time series for each of the 3104 sources can be retrieved from the *Gaia* first data release archive[12] and other distribution nodes. The archives also provide tools for queries and to cross-match *Gaia* data with other catalogues available in the literature.

We provide in Table 3 specific links to the archive tables, and summarise the names of the parameters computed by SOS

Table 3. Links to *Gaia* archive tables to retrieve the G-band time series photometry and the pulsation characteristics: period, epoch of maximum light (E), peak-to-peak G amplitude [Amp(G)], intensity-averaged mean G magnitude, ϕ_{21}, R_{21} Fourier parameters, and related uncertainties.

Table URL	http://archives.esac.esa.int/gaia/
G-band time series data	
Table name	phot_variable_time_series_gfov
Table content	G-band FoV averaged photometry: observation_time, g_flux, g_flux_error, g_magnitude, rejected_by_variability_processing
Table name	phot_variable_time_series_gfov_statistical_parameters
N_{obs}	num_observations_processed
Cepheid parameters computed by the SOS Cep&RRL pipeline	
Table name	**cepheid**
Source ID	source_id
Type	type_best_classification (one of DCEP, T2CEP or ACEP)
Mode	mode_best_classification (one of FUNDAMENTAL, FIRST_OVERTONE, SECOND_OVERTONE, or UNDEFINED, only for DCEP or ACEP)
Subtype	type2_best_sub_classification (BL_HER, W_VIR, or RV_TAU, only for T2CEP)
P	p1
$\sigma(P)$	p1_error
N_{harm}	num_harmonics_for_p1
E[a]	epoch_g
σE	epoch_g_error
$\langle G\rangle$	int_average_g
$\sigma\langle G\rangle$	int_average_g_error
Amp(G)	peak_to_peak_g
σ[Amp(G)]	peak_to_peak_g_error
ϕ_{21}	phi21_g
$\sigma(\phi_{21})$	phi21_g_error
R_{21}	r21_g
$\sigma(R_{21})$	r21_g_error
RR Lyrae star parameters computed by the SOS Cep&RRL pipeline	
Table name	**rrlyrae**
Source ID	source_id
Type	best_classification (one of RRC or RRAB)
P	p1
$\sigma(P)$	p1_error
N_{harm}	num_harmonics_for_p1
E[a]	epoch_g
σE	epoch_g_error
$\langle G\rangle$	int_average_g
$\sigma\langle G\rangle$	int_average_g_error
Amp(G)	peak_to_peak_g
σ[Amp(G)]	peak_to_peak_g_error
ϕ_{21}	phi21_g
$\sigma(\phi_{21})$	phi21_g_error
R_{21}	r21_g
$\sigma(R_{21})$	r21_g_error

Notes. Values were computed by the SOS Cep&RRL pipeline for the 599 Cepheids and 2595 RR Lyrae stars published in *Gaia* DR1. To ease the data retrieval, we also provide the correspondence between parameter (period, E, etc.) and the name of the parameter in the *Gaia* archive table. [(a)] The BJD of the epoch of maximum light is offset by JD 2 455 197.5 d (= J2010.0).

[12] http://archives.esac.esa.int/gaia/

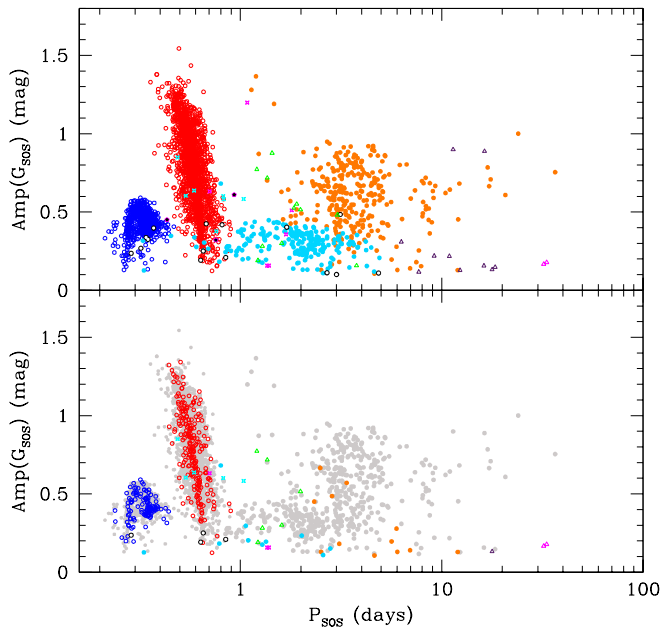

Fig. 18. Period-*G*-band amplitude diagram of the Cepheids and RR Lyrae stars published in *Gaia* DR1. The *upper panel* shows all 3194 sources; symbols and colour-coding are as in Fig. 17. In the *lower panel* new discoveries by *Gaia* are plotted in colour, known variables in grey.

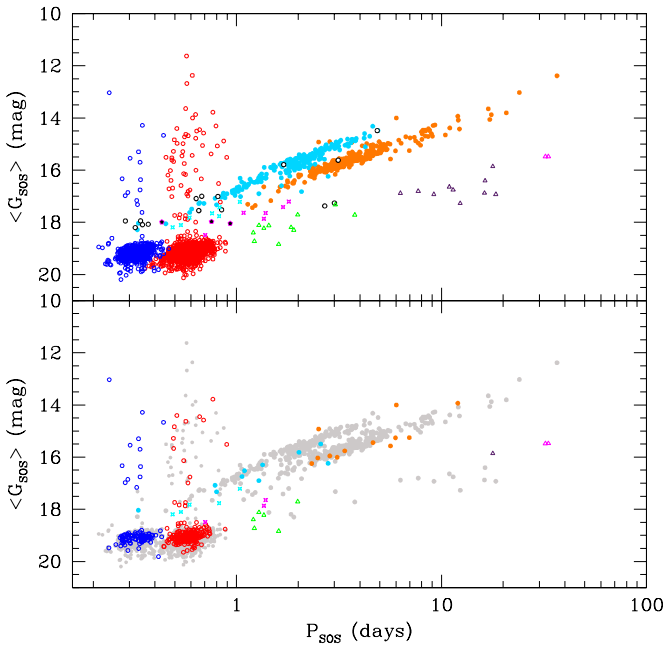

Fig. 19. *G*-band *PL* distribution of the 3194 Cepheids and RR Lyrae published in *Gaia* DR1. The *upper panel* shows all 3194 sources; symbols and colour coding are as in Fig. 17. In the *lower panel* new discoveries by *Gaia* are plotted in colour, known variables in grey.

Cep&RRL that can be retrieved from the archive tables. In Appendix B we provide queries to retrieve the various quantities and parameters listed in Table 3.

The *PA* and *PL* distributions of the total sample of 3194 sources are shown in Figs. 18 and 19, whereas Figs. 21 and 22 show their distribution in the Fourier ϕ_{21} vs. P and R_{21} vs. P planes, respectively, according to the period determined by the SOS Cep&RRL pipeline ($P_{\rm SOS}$). The MW RR Lyrae stars are clearly recognised in Fig. 19 for $P < 1$ d. This figure also shows the overlap between RR Lyrae stars, DCEPs, and ACEPs, occurring in the short period regime ($P < 1$d). Of the 3194 Cepheids and RR Lyrae stars published in *Gaia* DR1, 2808 are already known. Figure 20 shows the comparison with the literature. The comparison is done primarily with OGLE, for which there is the largest number of sources in common (2659 out of the 2808 known RR Lyrae stars and Cepheids). Other surveys among those listed at the end of Sect. 3.1 were considered in case an OGLE classification was not available. Since contrasting classifications were manually checked during the processing, the number of sources in Fig. 20 for which the SOS Cep&RRL classification differs from the literature is limited and reflects actual differences resulting from the analysis based on *Gaia* data.

Examples of light curves for RR Lyrae stars and Cepheids released in *Gaia* DR1 are presented in Figs. 23 and 24. Light curves are folded according to period and epoch of maximum light determined by the SOS Cep&RRL pipeline. The full atlas of light curves is available at `http://davide2.bo.astro.it/~felix/`. Samplers are shown in Appendices C and D, for Cepheids and RR Lyrae stars, respectively. New discoveries by *Gaia* are labelled.

Classical Cepheids with periods ranging from about 6 to 16 d show a secondary maximum (bump) in their light and RV curves, whose position varies with the pulsation period (see Bono et al. 2000 for details). This phenomenon is called the Hertzsprung progression (Hertzsprung 1926; Ledoux & Walraven 1958).

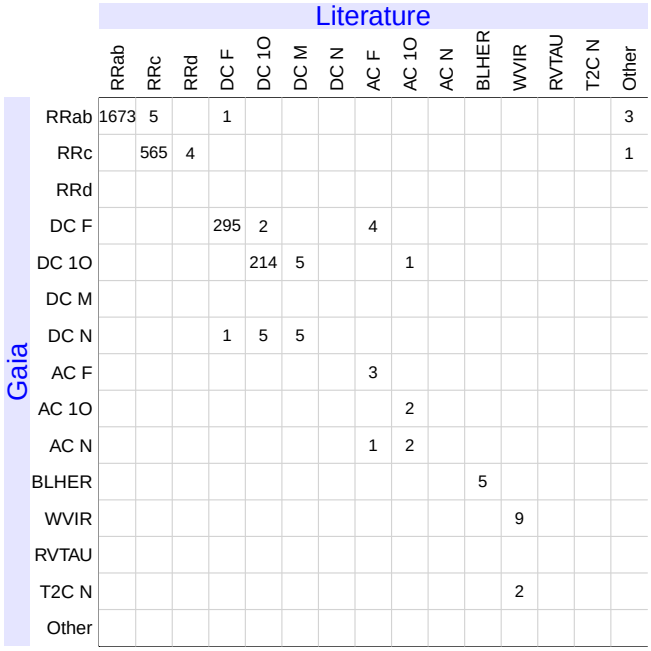

Fig. 20. Confusion matrix of the comparison with the literature for 2808 known Cepheids and RR Lyrae stars published in *Gaia* DR1. Rows refer to results of the SOS Cep&RRL pipeline and columns to literature results. DC, AC, and T2C indicate, respectively, DCEPs, ACEPs, and T2CEPs; DC M indicates multi-mode DCEPs. DC N, AC N, and T2C N indicate, respectively, DCEPs and ACEPs for which the pulsation mode was not identified and T2CEPs for which the subtype was not identified.

In the case of Galactic DCEPs the bump appears on the descending branch of the light and RV curves for $P < 9$ d, close to maximum light for $9 < P < 12$ d, and along the rising branch for longer periods. The period at the centre of the Hertzsprung progression varies with metallicity moving to longer periods

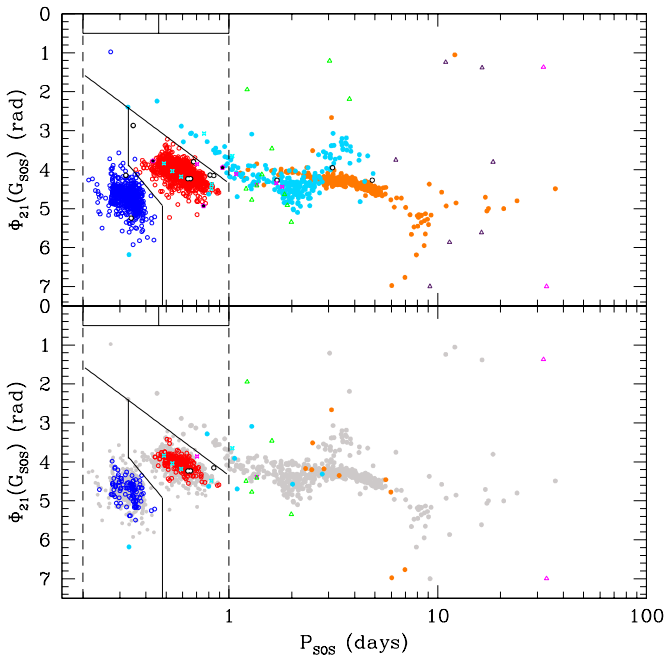

Fig. 21. ϕ_{21} vs. P_{SOS} distribution of the 3194 Cepheids and RR Lyrae stars published in *Gaia* DR1. Solid and dashed lines show the loci that were set in the SOS Cep&RRL pipeline to separate RR Lyrae stars from Cepheids and RRc from RRab pulsators. The *upper panel* shows all 3194 sources; symbols and colour-coding are as in Fig. 17. In the *lower panel* new discoveries by *Gaia* are plotted in colour, known variables in grey.

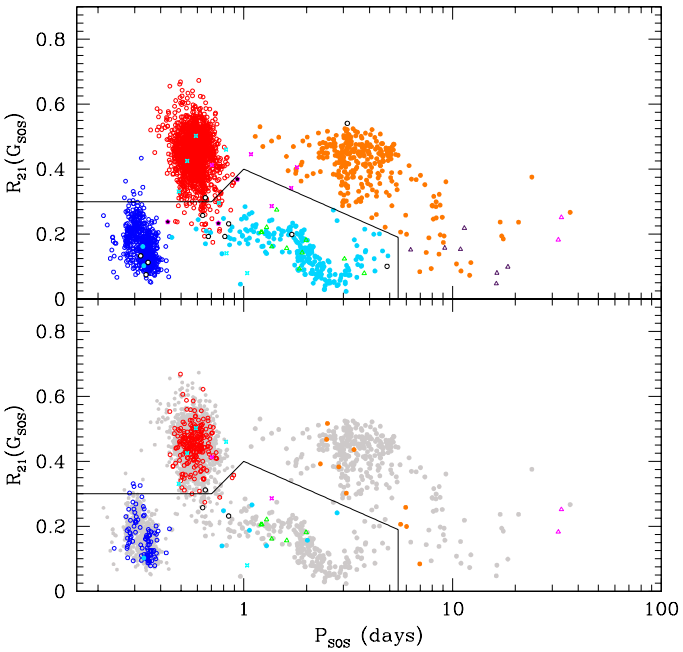

Fig. 22. R_{21} vs. P_{SOS} distribution of the 3194 Cepheids and RR Lyrae stars published in *Gaia* DR1. Solid and dashed lines show the loci that were set in the SOS Cep&RRL pipeline to separate RR Lyrae stars from Cepheids and to identify the Cepheid pulsation mode. The *upper panel* shows all 3194 sources; symbols and colour-coding are as in Fig. 17. In the *lower panel* new discoveries by *Gaia* are plotted in colour, known variables in grey.

as metallicity decreases (Marconi et al. 2005; Soszynski et al. 2011a). Figure 25 shows the *G*-band light curves for a subset of DCEPs that exhibit the Hertzsprung progression. The centre of the progression for these DCEPs is close to 9 days, as it is for the MW DCEPs, thus possibly suggesting that their metallicity is higher than for the bulk of the LMC Cepheids.

Figures 26 and 27 show, respectively, the number of observations available for the 2595 SEP RR Lyrae stars and the 599 Cepheids in *Gaia* DR1. The distribution peaks between 40 and 70 with a maximum of around 50 transits for the RR Lyrae stars and between 60 and 80 with a maximum of around 70 transits for the Cepheids, which means that these SEP sources provide a reasonably realistic representation of the typical number of observations per source that will be available on average at the end of the five-year nominal lifetime of the *Gaia* mission, although with a totally different cadence. However, we note that for the specific case of regular, periodic objects with typical periods of RR Lyrae stars and Cepheids and over a large time interval (e.g. the five-year time span), the sparser NSL cadence being less prone to aliasing than the EPSL cadence, whose sampling is too regular, may turn into an advantage for period derivation.

Figures 28 and 29 show the period distributions of the RR Lyrae stars and Cepheids in *Gaia* DR1. In both figures the light blue shaded areas correspond to new discoveries by *Gaia*. New and known variables follow very similar distributions. The RR Lyrae stars show the typical bimodal distribution corresponding to RRc and RRab pulsators. The period distribution of the RRab stars peaks at $P \sim 0.59$ d and confirms a predominantly Oosterhoff-intermediate nature of the LMC RR Lyrae stars (Oosterhoff 1939; Catelan 2009, and references therein). However, a minor component of Oosterhoff type II RRab stars is also present, which defines a second less populated sequence in the *PA* diagram shown in Fig. 30.

Figure 31 shows the *PL* distribution of the 2595 SEP RR Lyrae stars. The LMC RR Lyrae stars in the *Gaia* SEP typically appear to have $\langle G \rangle \sim 19.0$ mag with a dispersion of about ± 0.5 mag. This rather large dispersion is due to the combination of *PL* intrinsic width, reddening, metallicity effects, LMC geometric depth, and also to the extended throughput of *Gaia* *G*-band (330−1050 nm), which means that the RR Lyrae star *PL* relation has a significant span in the *G*-band (Gaia Collaboration 2016b). On the other hand, the over six magnitudes scatter seen in Fig. 31 for $G \sim 18$ mag is largely due to Galactic RR Lyrae stars that fall within the *Gaia* SEP footprint and contaminate the LMC sample.

Figure 32 shows the spatial distribution of the 2595 RR Lyrae stars in *Gaia* DR1 overlaid on the sample of LMC RR Lyrae stars recently released by OGLE-IV (Soszynski et al. 2016, orange filled circles). Marked in green are the RR Lyrae stars observed by *Gaia* that are in common with other surveys listed at the end of Sect. 3.1. About 700 of them were new discoveries by *Gaia* that were in the meantime also identified by OGLE (Soszynski et al. 2016). Red filled circles are 343 new RR Lyrae stars discovered by *Gaia*; they mainly belong to the LMC and allow a first glance at the very extended halo of this galaxy. Also particularly interesting is the distribution in average magnitude of the 2595 RR Lyrae stars in the *Gaia* SEP. This is shown in Fig. 33, where we have sliced the sample into three magnitude bins. The top panel shows 73 RR Lyrae stars with $\langle G \rangle < 18.5$ mag, sixty-three of them have $\langle G \rangle < 17.5$ mag and 24 in this brighter sample are new discoveries by *Gaia*. All RR Lyrae stars in this panel likely belong to the MW halo in front of the LMC. The central panel shows 2375 RR Lyrae stars

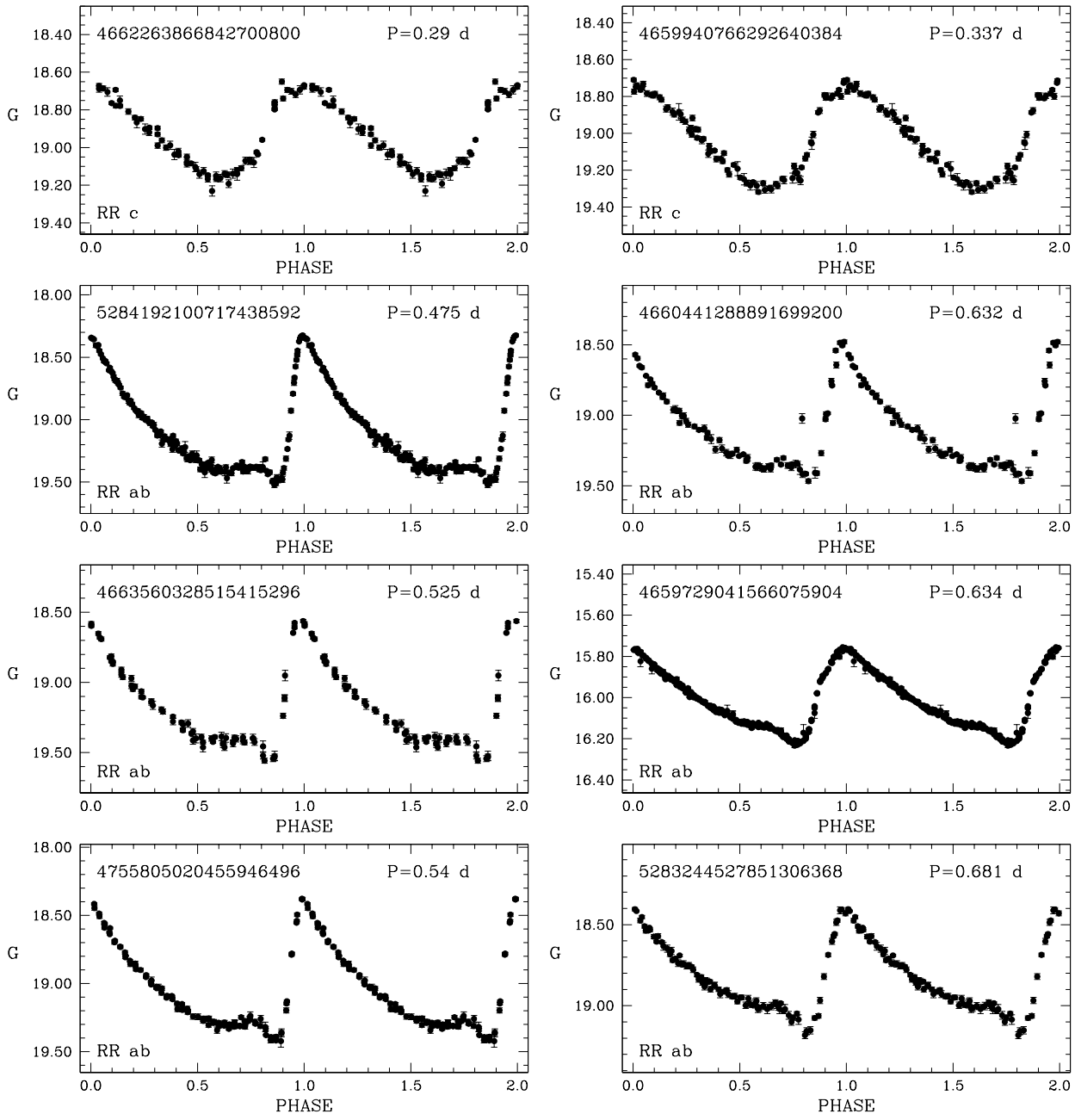

Fig. 23. Examples of *G*-band light curves of RRc (*top two panels*) and RRab stars in the LMC and in the MW halo (*third panel on the right*). Typical errors of individual measures at the magnitude level of the LMC RR Lyrae stars are of the order of $\gtrsim$0.02 mag. A few measurements with errors larger than 0.05 mag are not displayed.

with $18.5 < \langle G \rangle < 19.5$ mag. The average apparent magnitude of this sample is $\langle G \rangle = 19.13$ mag, with $\sigma = 0.16$ mag; this value is typical of the LMC RR Lyrae stars. They are quite homogeneously distributed and trace the LMC halo (see Fig. 32). The bottom panel shows 147 RR Lyrae stars with $\langle G \rangle > 19.5$ mag; they follow the clumped distribution of the LMC Cepheids in this area (see Fig. 35) and are fainter than the average of LMC RR Lyrae stars likely because they are more affected by reddening, which is expected to be higher in the dusty regions populated by Cepheids. This figure very nicely showcases the potential of *Gaia* and variable stars for studying galactic structure.

Finally, Figs. 34 and 35 show, respectively, the *PL* relation and the distribution on the sky of the 599 Cepheids in *Gaia* DR1. The various types of Cepheids in the sample clearly define different *PL* relations. They will be used to identify and classify different types of Cepheids in future *Gaia* data releases (see Sect. 5). Red filled circles in Fig. 35 mark 43 new Cepheids discovered by *Gaia*. This sample comprises 25 DCEPs, 10 ACEPs, and 8 T2CEPs which are located outside the OGLE-IV footprint and at increasing distance from the LMC. According to the position on the *PL* relation shown in Fig. 34 they belong to the LMC. However, it is premature to draw any conclusions on the LMC structure from this fairly small sample of new Cepheids, which might also be contaminated at the 3% level by ECLs (see Moretti et al. 2014), and by other types of variables (e.g. ellipsoidals or spotted stars) that populate the same period, period-luminosity, period-amplitude, and Fourier parameter domain. Whether some of these misclassifications may have

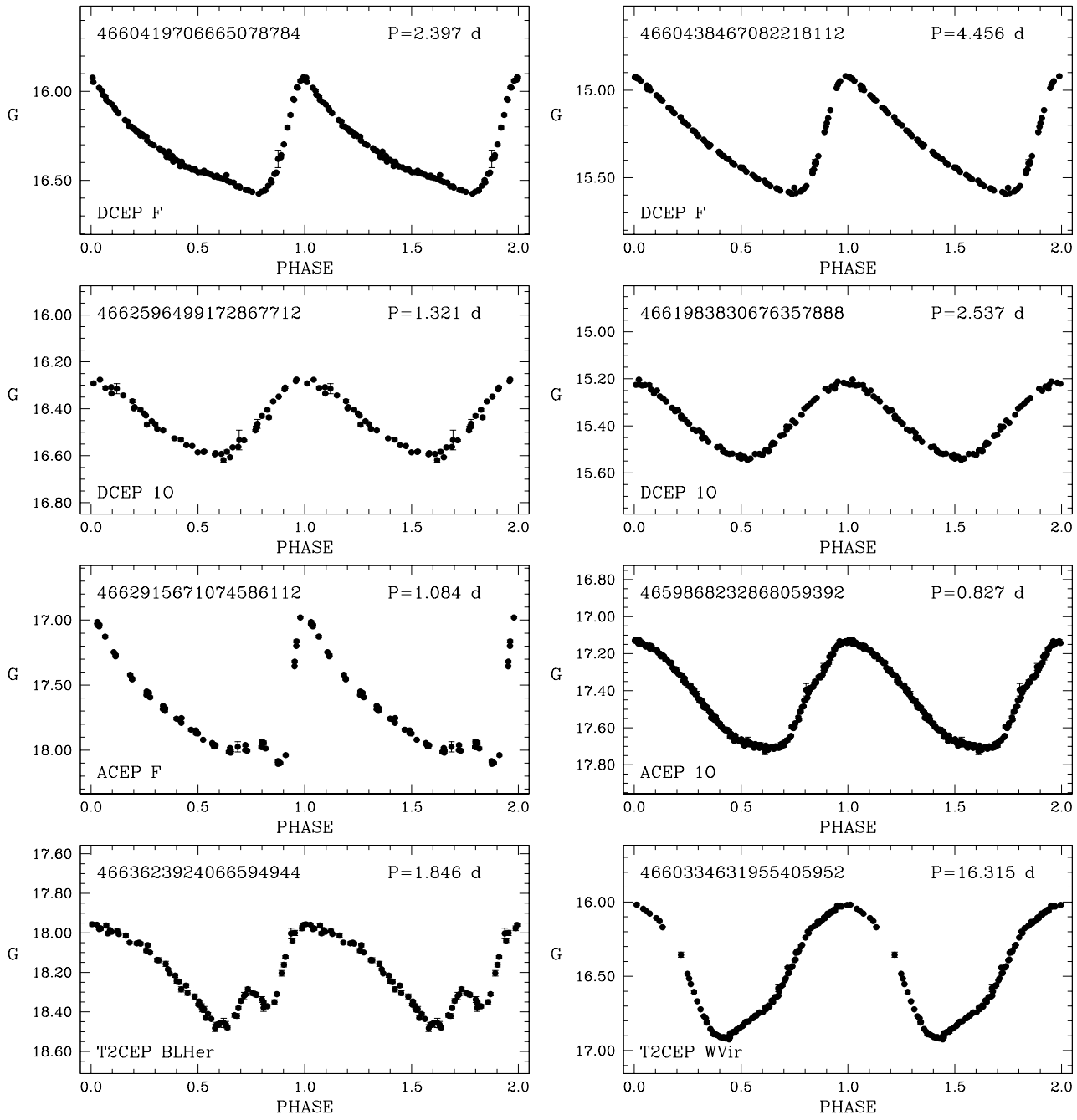

Fig. 24. *G*-band light curves of Cepheids of different type and pulsation mode released in *Gaia* DR1. *Top panels*: DCEPs F (*top two panels*); DCEPs 1O (*mid-upper two panels*); ACEP F (*mid-lower-left panel*), ACEP 1O (*mid-lower-right panel*); T2CEP BLHER (*lower-left panel*) and T2CEP WVIR (*lower-right panel*). Error bars are comparable to or smaller than symbol size.

actually occurred cannot be judged from the *Gaia* DR1 data alone. This will become possible and checks will certainly be done, if and where appropriate, now that we have started the re-processing of all sources in preparation of *Gaia* DR2. For *Gaia* second data release our analysis will also be easier because other parts of the CU7 pipeline will be activated, those specifically devoted to binaries of different types (among which also ellipsoidals) and to spotted stars in particular. Furthermore, for *Gaia* DR2 we will also have G_{BP}, G_{RP} time series available to help us disentangle Cepheids and RR Lyrae stars from other types of variables. We leave any further discussion of this sample for *Gaia* DR2 when the analysis of Cepheid and RR Lyrae candidates extends beyond the SEP footprint and G_{BP},G_{RP} photometry is used to help with the Cepheid classification.

5. Conclusions and future developments

We have presented an overview of the Specific Objects Study (SOS) pipeline SOS Cep&RRL, developed in the context of Coordination Unit 7 (CU7) of the *Gaia* Data Processing and Analysis Consortium (DPAC) to validate and fully characterise Cepheids and RR Lyrae variables observed by the spacecraft. The SOS Cep&RRL pipeline was specifically tailored to analyse the *Gaia* *G*-band time series photometry of sources in the

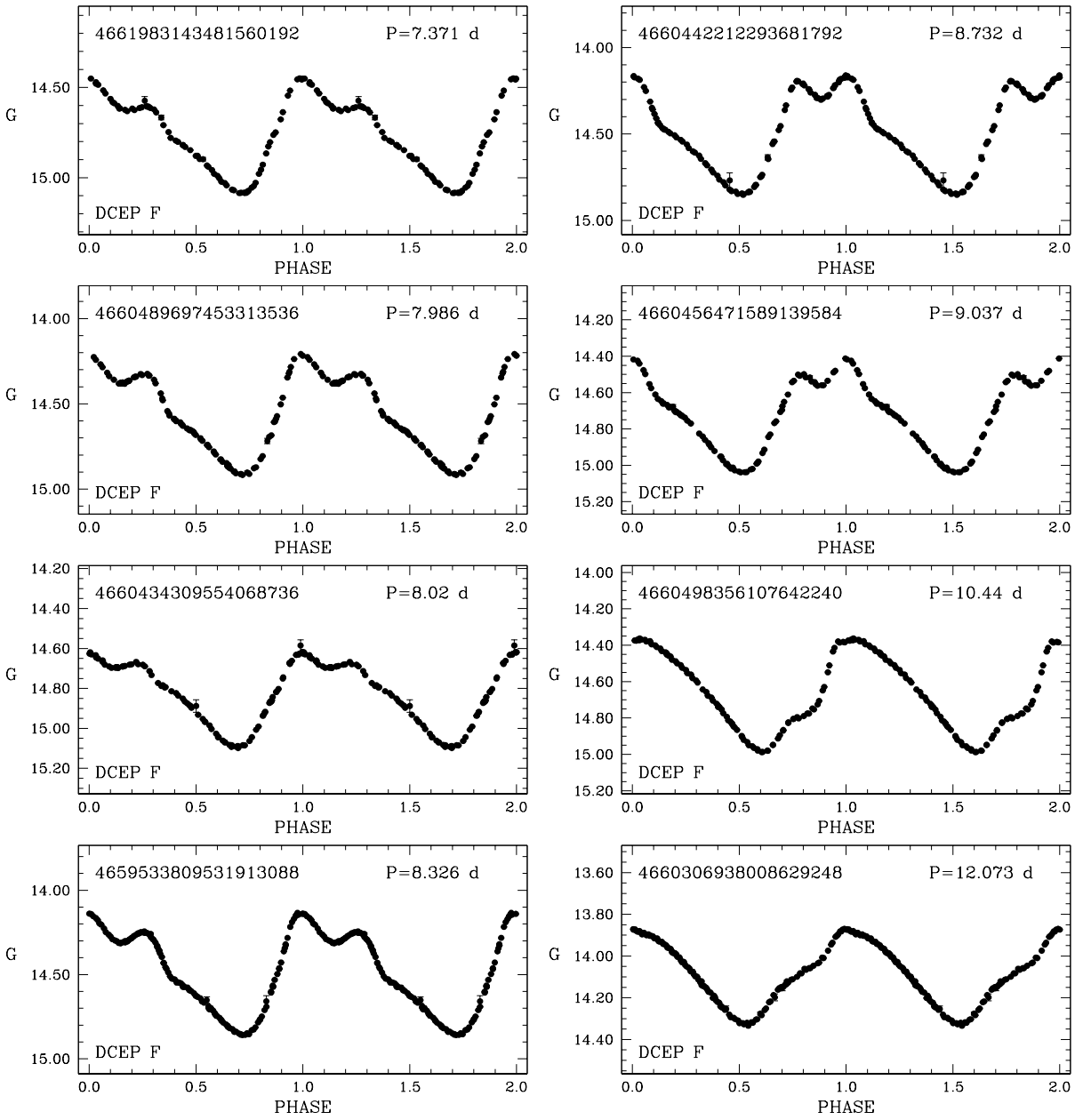

Fig. 25. *G*-band light curves of a subset of LMC DCEPs that exhibit the Hertzsprung progression. Error bars are comparable to or smaller than symbol size.

SEP footprint, which covers an external region of the LMC, and to produce results for confirmed RR Lyrae stars and Cepheids to be released with *Gaia* Data Release 1 (*Gaia* DR1).

The results presented in this paper were obtained by applying the whole variable star analysis pipeline on the time series photometry collected by *Gaia* during 28 days of ecliptic pole scanning law (EPSL) and 13 months of nominal scanning law (NSL). In addition to positions and *G*-band time series photometry, for confirmed Cepheids and RR Lyrae stars in the *Gaia* SEP, *Gaia* DR1 contains the following outputs of the SOS Cep&RRL pipeline: period of pulsation, classification in type and pulsation mode, intensity-averaged mean magnitude, peak-to-peak amplitude, and Fourier decomposition parameters R_{21} and ϕ_{21}. All quantities are provided with related uncertainties. The variable star inventory of *Gaia* DR1 includes 3194 variables which comprise 599 Cepheids and 2595 RR Lyrae stars, 386 of them (43 Cepheids and 343 RR Lyrae stars) are new discoveries by *Gaia*.

The published sources are distributed over an area extending 38 degrees on either side of a point offset from the centre of the LMC by about 3 degrees to the north and 4 degrees to the east. The vast majority are located within the LMC. The sample also includes 63 bright RR Lyrae stars that belong to the MW halo, of which 24 are new *Gaia* discoveries.

A number of improvements of the SOS Cep&RRL pipeline are planned in view of *Gaia* forthcoming releases. They include the following:

1. Passband transformations will be checked. In preparation for *Gaia* DR2, all tools and relations used by SOS Cep&RRL to classify and characterise the *Gaia* sources will be re-derived directly from Cepheids and RR Lyrae stars released

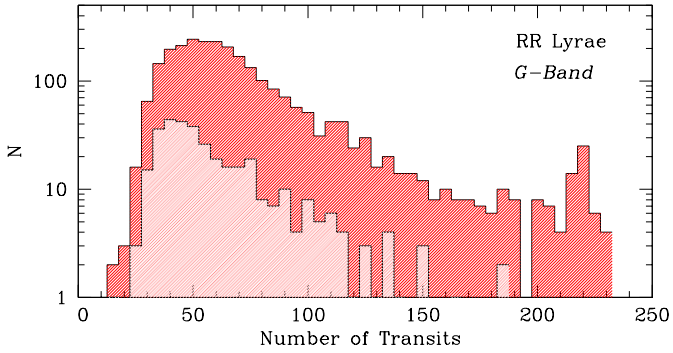

Fig. 26. Histogram showing the number of observations available for the 2595 SEP RR Lyrae stars published in *Gaia* DR1. The pink area shows the number of observations available for 343 new RR Lyrae stars in the sample.

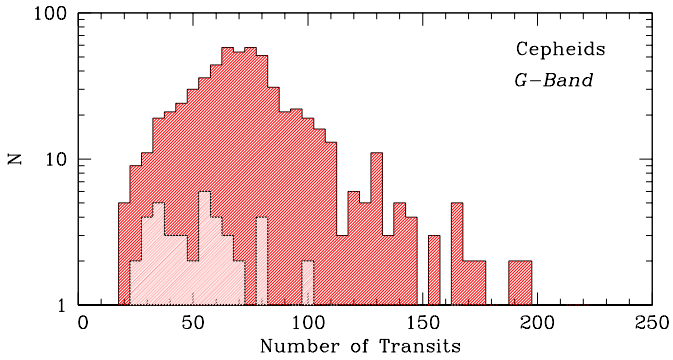

Fig. 27. Histogram showing the number of observations available for the 599 Cepheids published in *Gaia* DR1. The pink area shows the number of observations available for 43 new Cepheids in the sample.

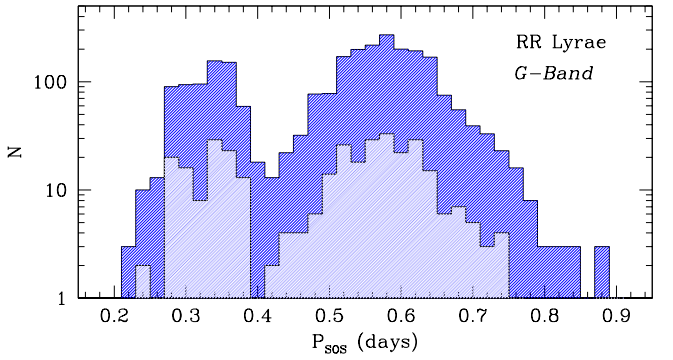

Fig. 28. Histogram showing the period distribution of the 2595 SEP RR Lyrae stars published in *Gaia* DR1. The light blue area shows the period distribution of 343 RR Lyrae stars that are new discoveries by *Gaia*.

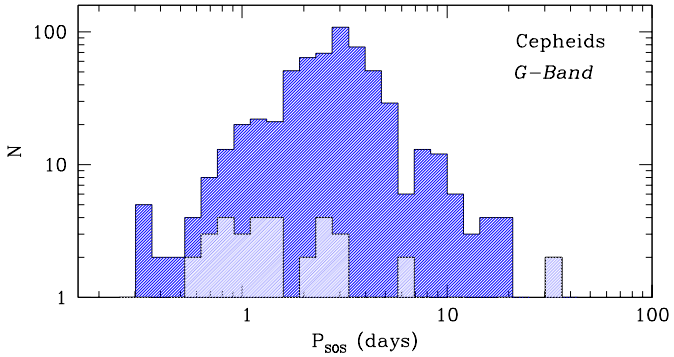

Fig. 29. Histogram showing the period distribution of the 599 Cepheids published in *Gaia* DR1. The light blue area shows the period distribution of 43 Cepheids in the sample that are new discoveries by *Gaia*.

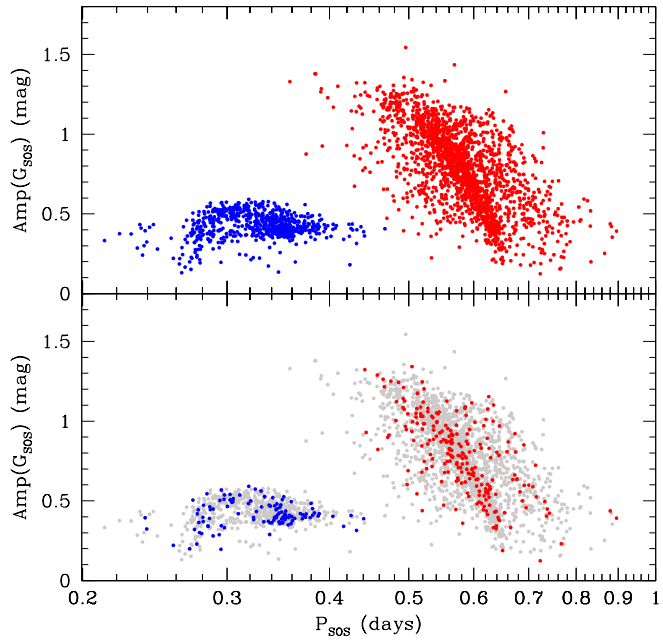

Fig. 30. Period-*G* amplitude diagram of the 2595 SEP RR Lyrae stars published in *Gaia* DR1. Blue and red filled circles indicate RRc and RRab pulsators, respectively. The *upper panel* shows the total sample of 2595 RR Lyrae stars. In the *lower panel* plotted in colour are the new RRab (red) and RRc (blue) stars discovered by *Gaia* (343 in total); the grey filled circles are the known RR Lyrae stars.

in DR1, overcoming the need for transforming quantities that are generally known in the Johnson-Cousins system to *Gaia* passbands. This will definitely allow the *PL* relationships adopted to identify and classify different types of Cepheids to be refined. On the other hand, as shown by Fig. A.2, the *G*-band transformation (Eq. (A.1)) worked rather well for the colour range spanned by the Cepheids and RR Lyrae stars in *Gaia* DR1.

2. *Gaia* G_{BP}, G_{RP} colours will become available with *Gaia* DR2. This will allow *PW* relations to be used; the reduced scatter, compared to the *PL* relations, will allow further improvement of the classification of Cepheids.
3. Double-mode RR Lyrae stars and multi-mode classical Cepheids (F/1O, 1O/2O, etc.) will be identified and fully characterised for *Gaia* DR2 by improving the detection algorithm to properly take into account the scatter in the folded light curve, thus reducing the number of false positives.
4. Estimate of the error in period, mean magnitude, peak-to-peak amplitude, etc., will be refined. In particular, errors in the Fourier parameters ϕ_{ij} and R_{ij}, which are currently computed by propagation of the errors in ϕ_i, ϕ_j, R_i, and R_j, will be entirely computed via Monte Carlo simulations.

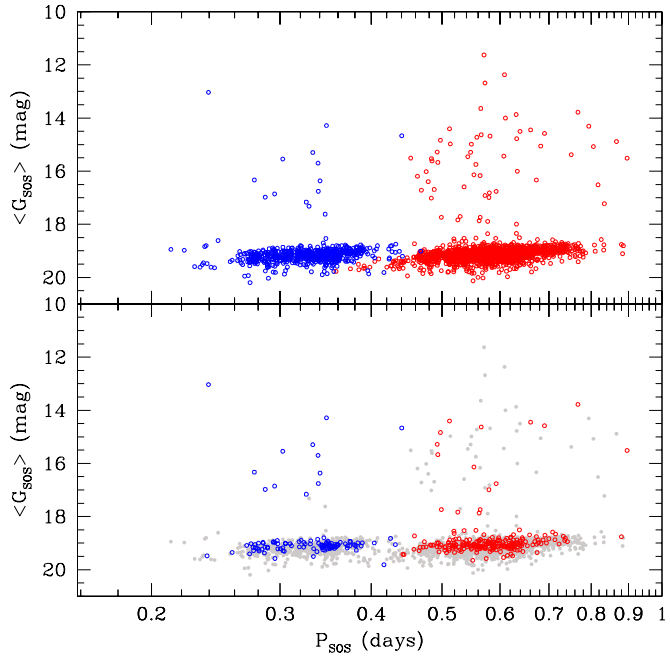

Fig. 31. *PL* distribution in the *G*-band of the SEP RR Lyrae stars published in *Gaia* DR1. Blue and red open circles indicate RRc and RRab pulsators, respectively. The *upper panel* shows the total sample of 2595 RR Lyrae stars. In the *lower panel* marked in blue and red are the new RR Lyrae stars discovered by *Gaia* (343 in total); the grey filled circles are the known RR Lyrae stars. RR Lyrae stars brighter than 18−18.5 mag likely belong to the MW halo in front of the LMC.

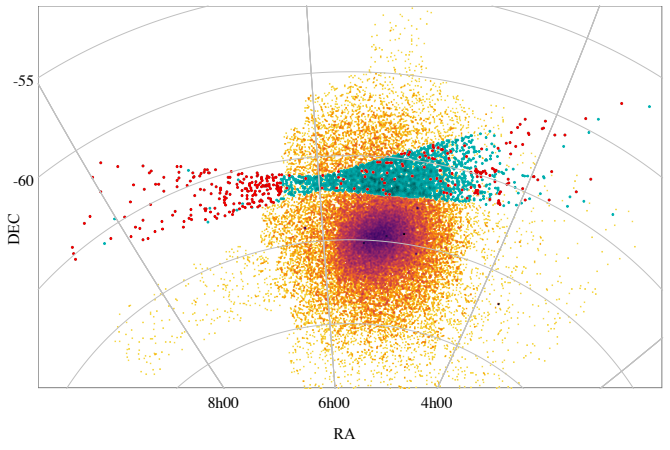

Fig. 32. Spatial distribution of the 2595 RR Lyrae stars released in *Gaia* DR1 compared with the distribution of LMC RR Lyrae stars from the OGLE-IV survey (orange dots; Soszynski et al. 2016). Green filled circles mark RR Lyrae stars observed by *Gaia* in common with other surveys (see text for details). Red filled circles are 343 new RR Lyrae stars discovered by *Gaia*.

5. A classifier will be developed to optimise the type and subtype classification of Cepheids and RR Lyrae stars performed by the SOS Cep&RRL pipeline.

The results for Cepheids and RR Lyrae stars shown in this paper demonstrate the excellent quality of *Gaia* photometry despite all the limitations in the dataset and processing for *Gaia* Data Release 1. They nicely showcase the potential of *Gaia* and the promise of *Gaia* Cepheids and RR Lyrae stars for all areas of the sky in which an appropriate light curve sampling will be achieved.

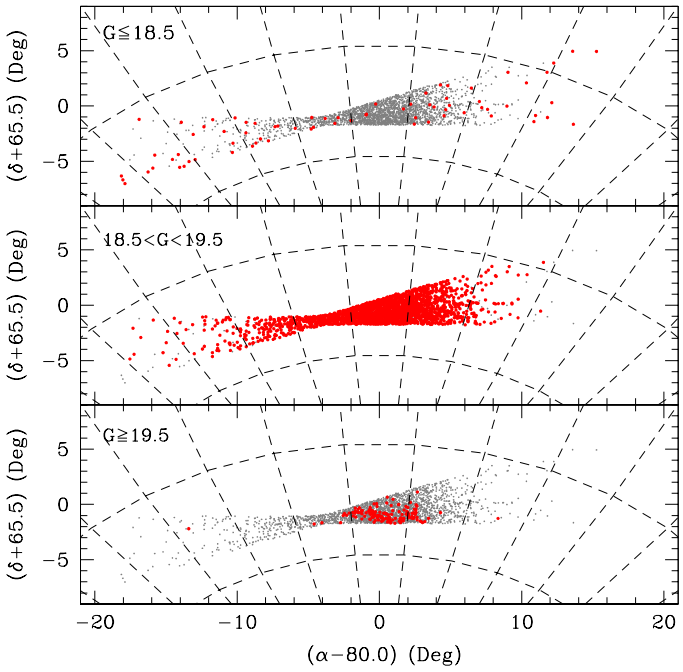

Fig. 33. Distribution on sky of the SEP RR Lyrae stars in *Gaia* DR1 according to their mean apparent *G*-band magnitude. The stars have been divided in three different magnitude ranges that are labelled in the figure.

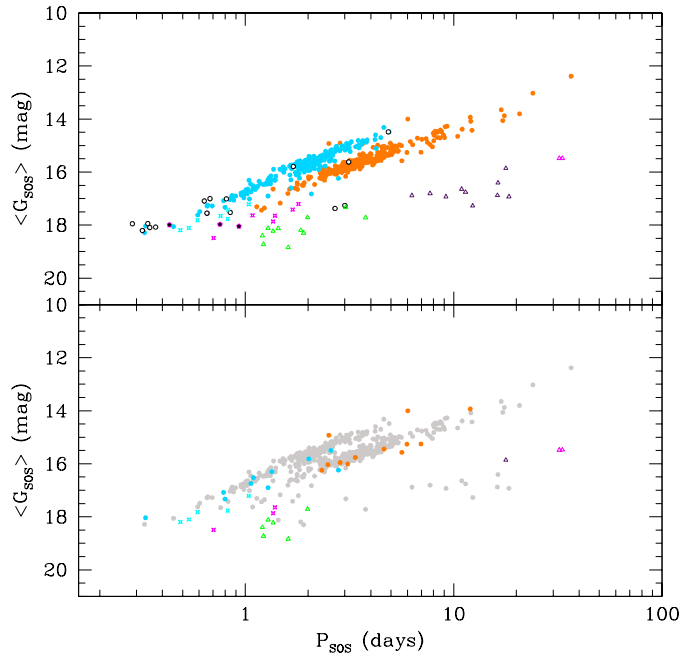

Fig. 34. *PL* distribution of the 599 Cepheids in *Gaia* DR1. Symbols and colour-coding are the same as in Fig. 17. The *upper panel* shows the total sample of 599 Cepheids. In the *lower panel* marked in colour are 43 new Cepheids discovered by *Gaia*. Grey filled circles are Cepheids already known.

Acknowledgements. This work has made use of data from the ESA space mission *Gaia*, processed by the *Gaia* Data Processing and Analysis Consortium (DPAC). Funding for the DPAC has been provided by national institutions

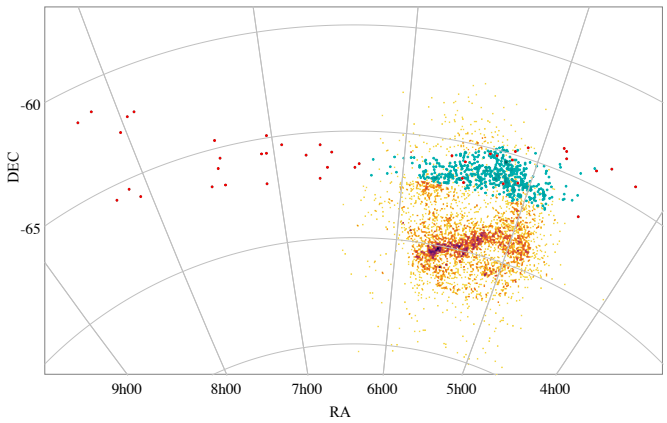

Fig. 35. Spatial distribution of the 599 Cepheids released in *Gaia* DR1, compared with the distribution of LMC Cepheids from the OGLE-IV survey (orange dots; Soszynski et al. 2015a,b,c). Green filled circles mark Cepheids observed by *Gaia* and already known from the OGLE and EROS-2 surveys. Red filled circles are 43 new Cepheids discovered by *Gaia*.

participating in the *Gaia* Multilateral Agreement. In particular, the Italian participation in DPAC has been supported by Istituto Nazionale di Astrofisica (INAF) and the Agenzia Spaziale Italiana (ASI) through grants I/037/08/0, I/058/10/0, 2014-025-R.0, and 2014-025-R.1.2015 to INAF (PI M. G. Lattanzi), the Belgian participation by the BELgian federal Science Policy (BELSPO) through PRODEX grants, the Swiss participation by the Swiss State Secretariat for Education, Research and Innovation through the ESA Prodex program, the "Mesures d'accompagnement", the "Activités Nationales Complémentaires", the Swiss National Science Foundation, and the Early Postdoc. Mobility fellowship, and the Spanish participation by the Spanish Ministry of Economy MINECO-FEDER through grants AyA2014-55216, AyA2011-24052. UK community participation in this work has been supported by funding from the UK Space Agency, and from the UK Science and Technology Research Council. The *Gaia* mission website is: `http://www.cosmos.esa.int/gaia`.

References

Bailey, S. I. 1902, Annals of Harvard College Observatory, 38, 1
Barnes, T. G., & Evans, D. S. 1976, MNRAS, 174, 489
Berdnikov, L. N., & Turner, D. G. 1995, Pis'ma Astr. Zhurnal, 21, 803
Berdnikov, L. N., Vozyakova, O. V., Kniazev, A. Y., et al. 2012, Astron. Rep., 56, 290
Berdnikov, L. N., Kniazev, A. Y., Sefako, R., Kravtsov, V. V., & Zhujko, S. V. 2014, Astron. Lett., 40, 125
Blazhko, S. 1907, Astr. Nachr., 175, 325
Bono, G., Marconi, M., & Stellingwerf, R. F. 2000, A&A, 360, 245
Cacciari, C., Clementini, G., Prevot, L., & Buser, R. 1989, A&A, 209, 141
Cacciari, C., Clementini, G., & Fernley, J. A. 1992, ApJ, 396, 219
Cacciari, C., Corwin, T. M., & Carney, B. W. 2005, AJ, 129, 267
Carrasco, J. M., Evans, D. W, Montegriffo, P., et al. 2016, A&A, 595, A7 (*Gaia* SI)
Catelan, M. 2009, Ap&SS, 320, 261
Clementini, G. 2016, in RR Lyrae 2015 – High-Precision Studies of RR Lyrae stars, eds. L. Szabados, R. Szabo, & K. Kinemuchi, Communications from the Konkoly Observatory of the Hungarian Academy of Sciences, 105, 3
Cohen, J. G., Sesar, B., Banholzer, S., et al. 2016, in Global Properties of Stellar Halos From the Milky Way to External Galaxies, IAU Symp., 317, 91
Coulson, I. M., & Caldwell, J. A. R. 1985, SAAO Circulars, 9, 5
Coulson, I. M., Caldwell, J. A. R., & Gieren, W. P. 1985, ApJS, 57, 595
Di Criscienzo, M., Marconi, M., & Caputo, F. 2004, ApJ, 612, 1092
Drake, A. J., Catelan, M., Djorgovski, S. G., et al. 2013, ApJ, 763, 32
Evans, D. W., Riello, M., De Angeli, F., et al. 2016, A&A, submitted (*Gaia* SI)
Eyer, L., Palaversa, L., Mowlavi, N., et al. 2012, Ap&SS, 341, 207
Eyer, L., Mowlavi, N., Evans, D. W., et al. 2016, A&A, submitted (*Gaia* SI)
Gaia Collaboration (Brown, A. G. A., et al.) 2016a, A&A, 595, A2 (*Gaia* SI)
Gaia Collaboration (Clementini, G., et al.) 2016b, A&A, submitted (*Gaia* SI)
Gaia Collaboration (Prusti, T., et al.) 2016c, A&A, 595, A1 (*Gaia* SI)
Gieren, W. 1981, ApJS, 47, 315
Hajdu, G., Catelan, M., Jurcsik, J., et al. 2015, MNRAS, 449, L113
Hernitschek, N., Schlafly, E. F., Sesar, B., et al. 2016, ApJ, 817, 73
Hertzsprung, E. 1926, Bull. Astron. Inst. Netherlands, 3, 115
Jordi, C., Gebran, M., Carrasco, J. M., et al. 2010, A&A, 523, A48
Kim, D.-W., Protopapas, P., Bailer-Jones, C. A. L., et al. 2014, A&A, 566, A43
Ledoux, P., & Walraven, T. 1958, Handbuch der Physik, 51, 353
Levenberg, K. 1944, Quarterly of Applied Mathematics, 2, 164
Lindegren, L., Lammers, U., Bastian, U., et al. 2016, A&A, 595, A4 (*Gaia* SI)
Liska, J., Skarka, M., Zejda, M., et al. 2015, MNRAS, 459, 4360
Lomb, N. R. 1976, Ap&SS, 39, 447
Marconi, M., Musella, I., & Fiorentino, G. 2005, ApJ, 632, 590
Marquardt, D. W. 1963, SIAM J. Appl. Math., 11, 431
Moffett, T. J., & Barnes, T. G. 1984, ApJS, 55, 389
Moretti, M. I., Clementini, G., Muraveva, T., et al. 2014, MNRAS, 437, 2702
Oosterhoff, P. T. 1939, Observatory, 62, 104
Osuna, P., Ortiz, I., Lusted, J., et al. 2008, IVOA Astronomical Data Query Language Version 2.00, IVOA Recommendation 30 October
Petersen, J. O. 1973, A&A, 27, 89
Pietrzyński, G., Graczyk, D., Gieren, W., et al. 2013, Nature, 495, 76
Pojmański, G. 1997, Acta Astron., 47, 467
Poleski, R., Soszyński, I., Udalski, A., et al., 2010, Acta Astron., 60, 179
Ripepi, V., Barone, F., Milano, L., & Russo, G. 1997, A&A, 318, 797
Scargle, J. D. 1982, ApJ, 263, 835
Sesar, B., Ivezić, Z., Stuart, J. S., et al. 2013, AJ, 146, 21
Soszyński, I., Poleski, R., Udalski, A., et al. 2008a, Acta Astron., 58, 163
Soszyński, I., Udalski, A., Szymański, M. K., et al. 2008b, Acta Astron., 58, 293
Soszyński, I., Udalski, A., Szymański, M. K., et al. 2009, Acta Astron., 59, 1
Soszyński, I., Poleski, R., Udalski, A., et al. 2010a, Acta Astron., 60, 17
Soszyński, I., Udalski, A., Szymański, M. K., et al. 2010b, Acta Astron., 60, 91
Soszyński, I., Udalski, A., Szymański, M. K., et al. 2010c, Acta Astron., 60, 165
Soszyński, I., Dziembowski, W. A., Udalski, A., et al. 2011a, Acta Astron., 61, 1
Soszyński, I., Udalski, A., Pietrukowicz, P., et al. 2011b, Acta Astron., 61, 285
Soszyński, I., Udalski, A., Poleski, R., et al. 2012, Acta Astron., 62, 219
Soszyński, I., Udalski, A., Szymański, M. K., et al. 2015a, Acta Astron., 65, 233
Soszyński, I., Udalski, A., Szymański, M. K., et al., 2015b, Acta Astron., 65, 297
Soszyński, I., Udalski, A., Szymański, M. K., et al., 2015c, Acta Astron., 65, 329
Soszyński, I., Udalski, A., Szymański, M. K., et al. 2016, Acta Astron., 66, 131
Torrealba, G., Catelan, M., Drake, A. J., et al. 2015, MNRAS, 446, 2251
van Leeuwen, F., De Angeli, F., Riello, M., et al. 2016, A&A, submitted (*Gaia* SI)
Wade, R. A., Donley, J., Fried, R., White, R. E., & Saha, A. 1999, AJ, 118, 2442
Walker, A. R. 1994, AJ, 108, 555

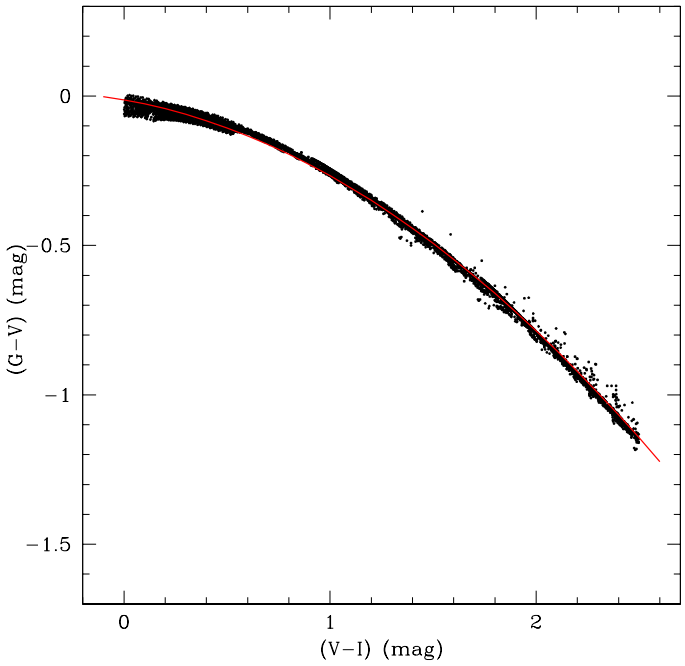

Fig. A.1. Conversion relation (red curve) used in the present paper to transform Johnson V, I to the *Gaia* G-band (Eq. (A.1)). The relation was computed by interpolating in the grid of models by Jordi et al. (2010) and subsequent updates (black solid points). New transformations have now been computed using *Gaia* real data (van Leeuwen et al. 2016); they supersede the formula provided here.

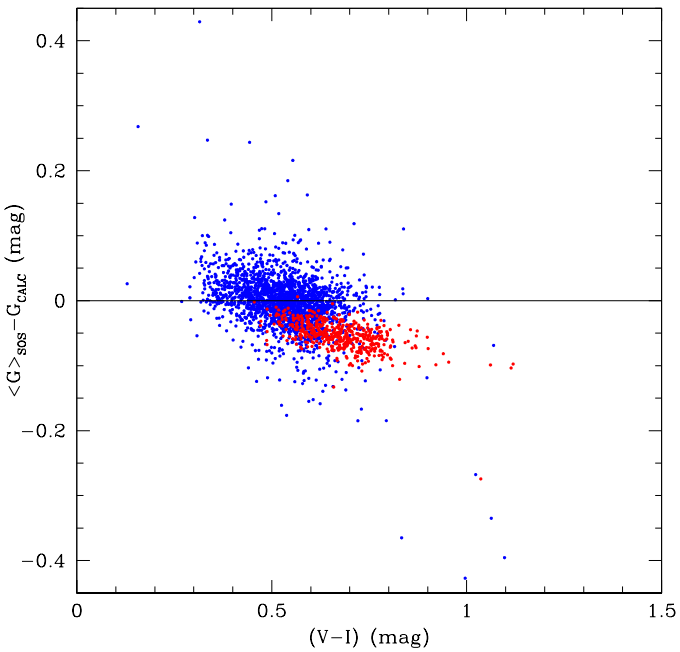

Fig. A.2. Comparison of the G-band mean magnitudes computed by the SOS Cep&RRL pipeline ($\langle G_{\rm SOS}\rangle$) for 510 Cepheids (red filled circles) and 2149 RR Lyrae stars (blue filled circles) in *Gaia* DR1 in common with the OGLE-IV survey and the values obtained transforming OGLE V, I mean magnitudes to the G-band using Eq. (A.1).

Appendix A: Conversion formula

In this section we present the conversion formula, appropriate for the colour and metallicity ranges of Cepheids and RR Lyrae stars ($V - I$ < 2.5 mag and −2.5 < [Fe/H] <0.5 dex), that we have used to transform the Johnson-Cousins V, I to the *Gaia* G passband. This formula was computed using passband transformations provided in Jordi et al. (2010) and subsequent updates (Jordi, priv. comm.):

$$G = V - (0.0128 \pm 0.0005) - (0.1218 \pm 0.0008)(V - I) - (0.1323 \pm 0.0003)(V - I)^2 \quad \text{rms} = 0.017 \text{ mag.} \quad \text{(A.1)}$$

The relation is shown by the red solid line in Fig. A.1.

It should be noted that the above conversion formula between the *Gaia* G and Johnson-Cousins V, I passbands is based on the pre-launch nominal *Gaia* G passband, hence it might not be perfect. Nevertheless, Fig. A.2 shows this transformation to have worked rather well for Cepheids and RR Lyrae stars that are published in *Gaia* DR1. In the figure we have plotted the $\langle G\rangle$ mean magnitude computed by the SOS Cep&RRL pipeline for 2659 sources (510 Cepheids and 2149 RR Lyrae stars) in common with OGLE-IV vs. the source $V - I$ colours from OGLE. The differences are, on average, within ±0.1 mag.

New transformations have now been computed using *Gaia* real data (van Leeuwen et al. 2016). The reader is advised to use the new formulae to make passband transformations. As far as future *Gaia* releases are concerned, Cepheids and RR Lyrae stars published in *Gaia* DR1 will be used to compute directly in the *Gaia* G-band the *PA* and *PL* relations used in the SOS Cep&RRL pipeline to classify these types of variable stars.

Appendix B: Examples of *Gaia* archive queries

Table B.1. Queries to retrieve information on the Cepheids and RR Lyrae stars from the *Gaia* archive in the Astronomical Data Query Language (Osuna et al. 2008).

Query to retrieve time series of all Cepheids in the *Gaia* DR1.

```
select gaia.source_id, gaia.observation_time, gaia.g_flux, gaia.g_flux_error,
  gaia.g_magnitude, gaia.rejected_by_variability_processing
from gaiadr1.phot_variable_time_series_gfov as gaia
inner join gaiadr1.cepheid as cep
  on gaia.source_id=cep.source_id
```

Query to retrive time series of all RR Lyrae stars in the *Gaia* DR1.

```
select gaia.source_id, gaia.observation_time, gaia.g_flux, gaia.g_flux_error,
  gaia.g_magnitude, gaia.rejected_by_variability_processing
from gaiadr1.phot_variable_time_series_gfov as gaia
inner join gaiadr1.rrlyrae as rr
  on gaia.source_id=rr.source_id
```

Query to retrieve the number of processed observations and SOS Cep&RRL-computed parameters of all Cepheids in the *Gaia* DR1.

```
select cep.source_id, num_observations_processed, type_best_classification,
  mode_best_classification, type2_best_sub_classification, p1, p1_error,
  num_harmonics_for_p1, epoch_g, epoch_g_error, int_average_g, int_average_g_error,
  peak_to_peak_g, peak_to_peak_g_error, phi21_g, phi21_g_error, r21_g, r21_g_error
from gaiadr1.phot_variable_time_series_gfov_statistical_parameters as stat
inner join gaiadr1.cepheid as cep
 on stat.source_id=cep.source_id
```

Query to retrieve the number of processed observations and SOS Cep&RRL-computed parameters of all RR Lyrae in the *Gaia* DR1.

```
select rr.source_id, num_observations_processed, best_classification, p1, p1_error,
  num_harmonics_for_p1, epoch_g, epoch_g_error, int_average_g, int_average_g_error,
  peak_to_peak_g, peak_to_peak_g_error, phi21_g, phi21_g_error, r21_g, r21_g_error
from gaiadr1.phot_variable_time_series_gfov_statistical_parameters as stat
inner join gaiadr1.rrlyrae as rr
  on stat.source_id=rr.source_id
```

Appendix C: Atlas of the *G*-band light curves for Cepheids

In this appendix we present the *G*-band light curves of 599 Cepheids observed by *Gaia* in the SEP region. The light curves are folded according to the period and epoch of maximum light computed by the SOS Cep&RRL pipeline and are plotted grouping the Cepheids by type and pulsation mode according to the following order: DCEPs 1O (230 in total), DECPs F (313), DCEPs NoMode (15 DCEPs for which we did not identify the pulsation mode); ACEPs 1O (7 sources), ACEPs F (6), ACEPs NoMode (3); T2CEPs BLHER (11 sources), T2CEPs WVIR (10), T2CEPs RVTAU (2), and T2CEPs NoMode (2). In each group the sources are displayed in order of increasing period.

Appendix D: Atlas of the *G*-band light curves for RR Lyrae stars

In this appendix we present the *G*-band light curves of 2595 RR Lyrae stars observed by *Gaia* in the SEP region. The light curves are folded according to the period and epoch of maximum light computed by the SOS Cep&RRL pipeline and are plotted grouping the RR Lyrae stars according to the pulsation mode: the 685 RRc stars are first, followed by the 1910 RRab stars. In each group the sources are displayed in order of increasing period.

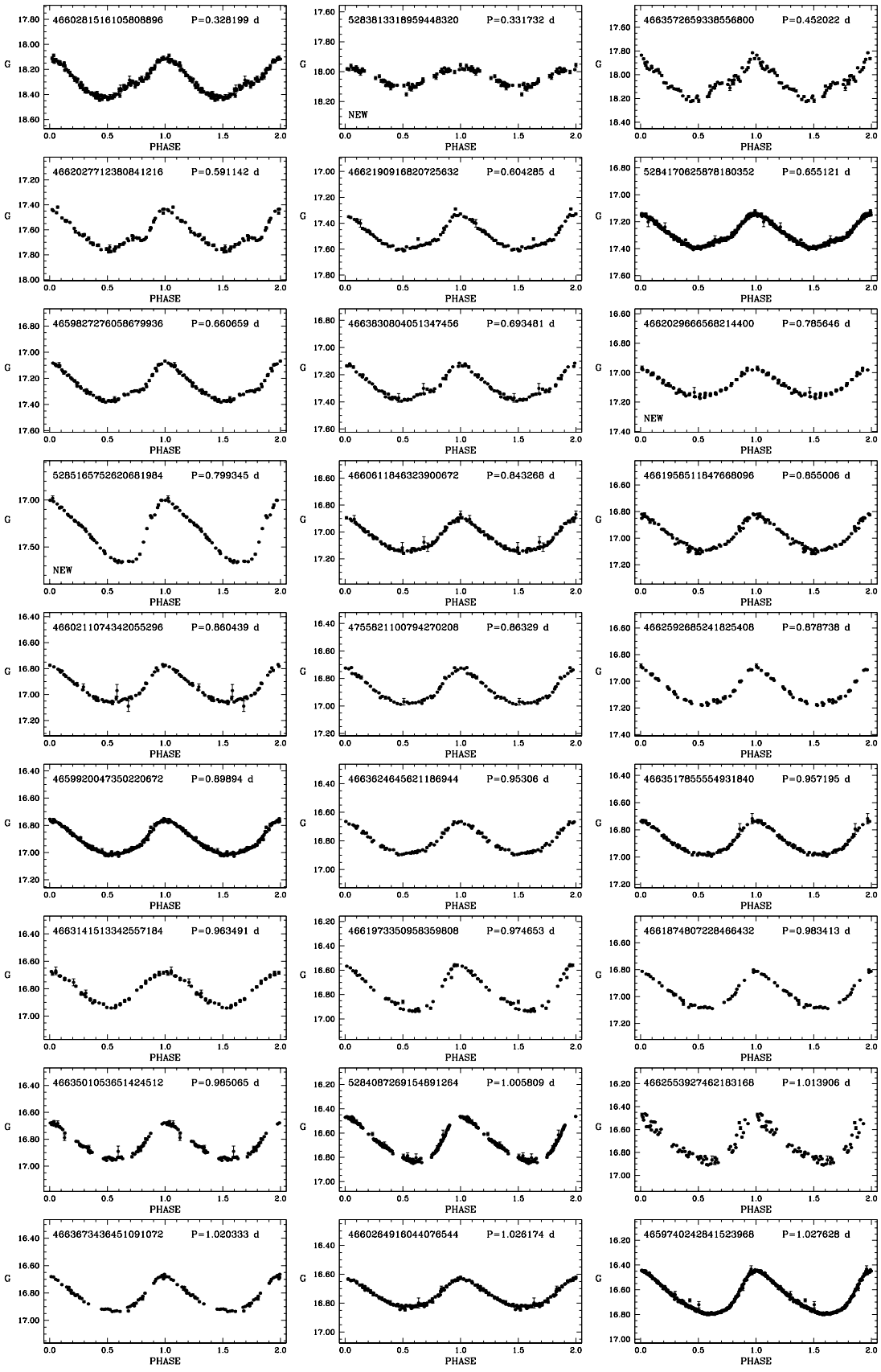

Fig. C.1. *G*-band light curves of first overtone DCEPs released in *Gaia* DR1 ordered by increasing period. Error bars are comparable to or smaller than the symbol size. Measurements with errors larger than 0.05 mag are not displayed. For each source we label the *Gaia* source ID and the pulsation period rounded to the last significant digit according to the error of the period determination. New discoveries by *Gaia* are flagged as such.

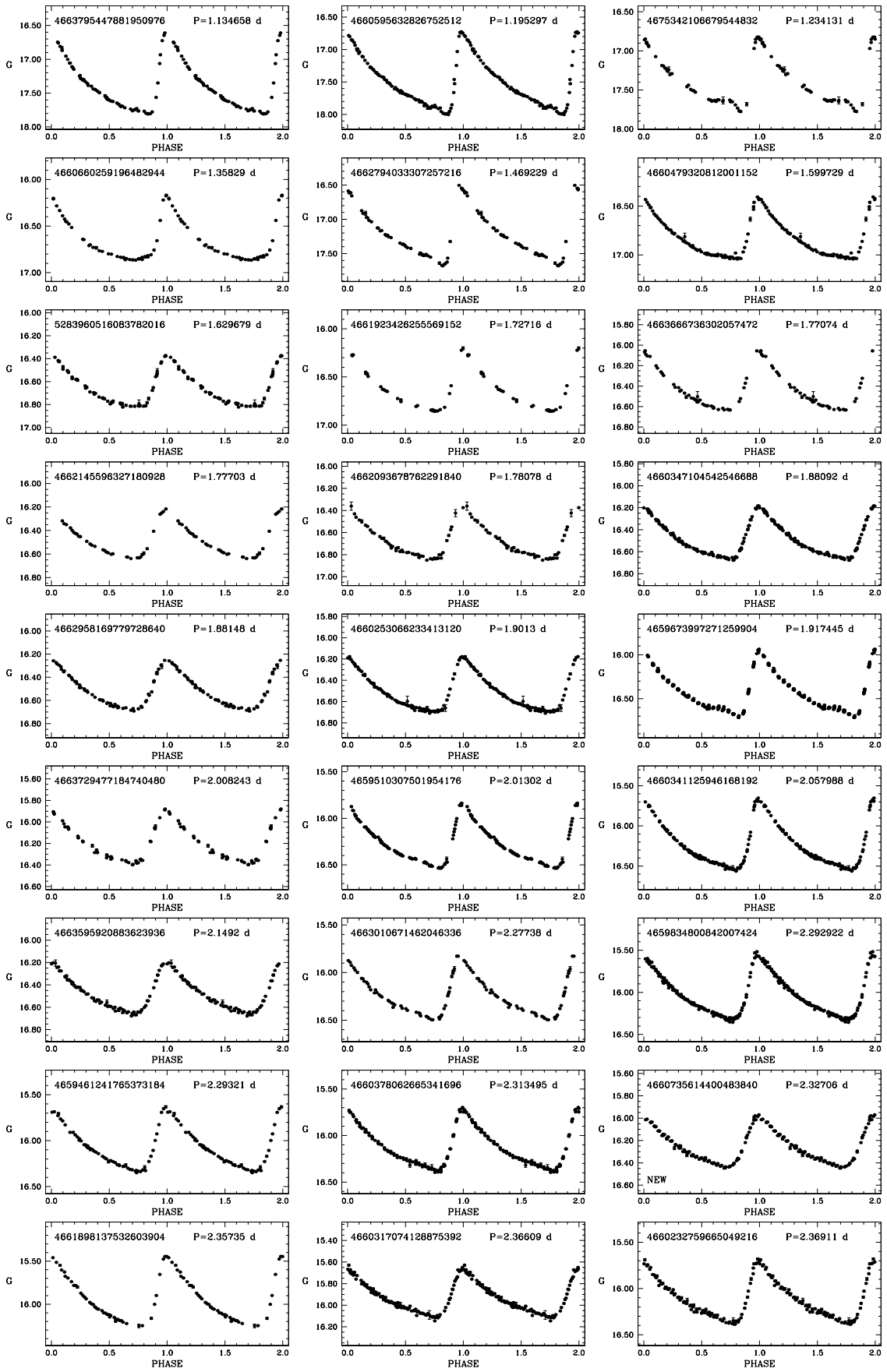

Fig. C.2. *G*-band light curves of fundamental mode DCEPs released in *Gaia* DR1 ordered by increasing period. Error bars are comparable to or smaller than the symbol size. Measurements with errors larger than 0.05 mag are not displayed. For each source we label the *Gaia* source ID and the pulsation period rounded to the last significant digit according to the error of the period determination. New discoveries by *Gaia* are flagged as such.

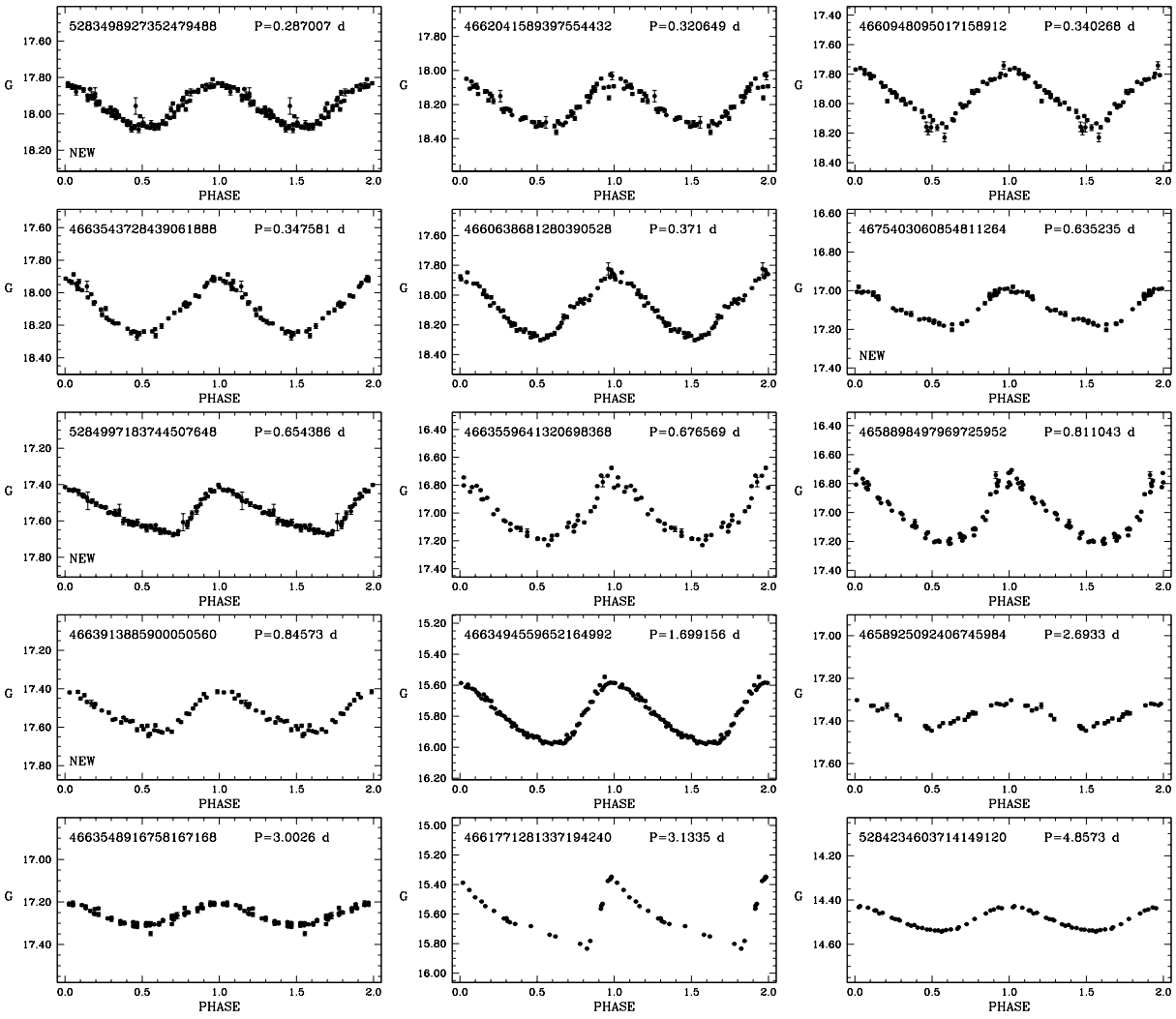

Fig. C.3. *G*-band light curves of DCEPs released in *Gaia* DR1 for which we did not identify the pulsation mode. Error bars are comparable to or smaller than the symbol size. Measurements with errors larger than 0.05 mag are not displayed. For each source we label the *Gaia* source ID and the pulsation period rounded to the last significant digit according to the error of the period determination. New discoveries by *Gaia* are flagged as such.

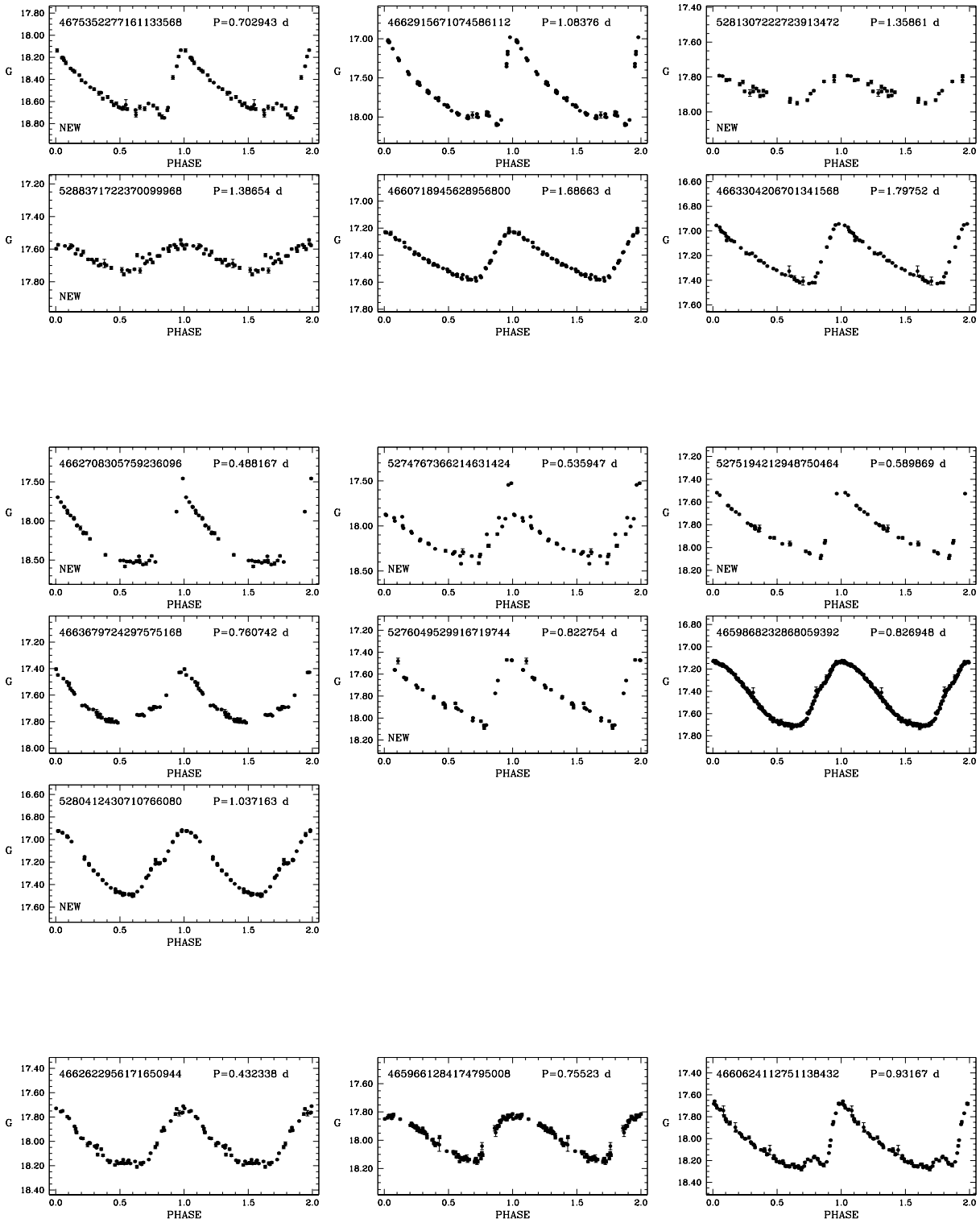

Fig. C.4. *G*-band light curves of ACEPs released in *Gaia* DR1 ordered by increasing period. *From top to bottom* ACEPs F, ACEPs FO, and ACEPs for which we did not identify the pulsation mode. Error bars are comparable to or smaller than the symbol size. Measurements with errors larger than 0.05 mag are not displayed. For each source we label the *Gaia* source ID and the pulsation period rounded to the last significant digit according to the error of the period determination. New discoveries by *Gaia* are flagged as such.

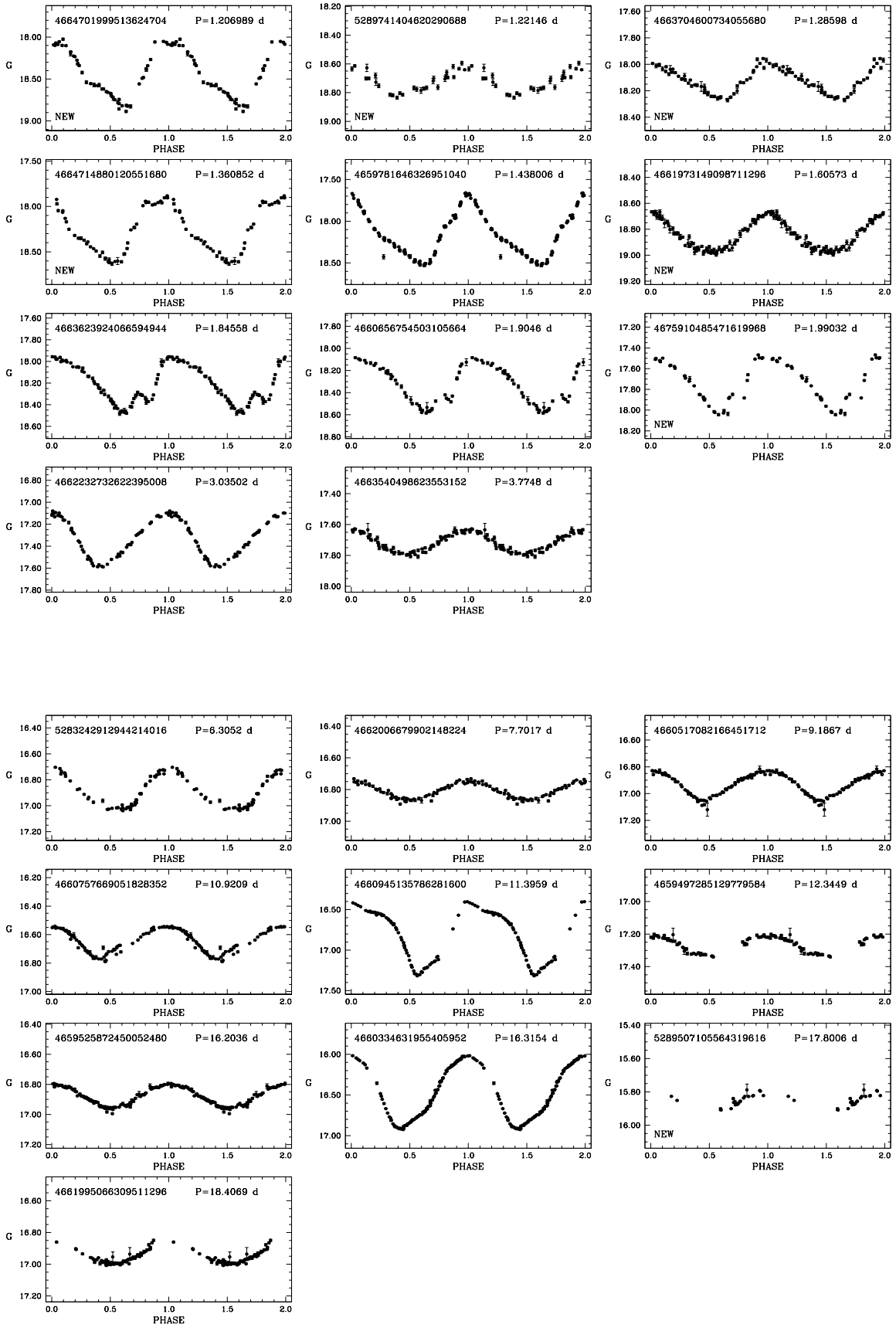

Fig. C.5. *G*-band light curves of T2CEPs released in *Gaia* DR1 ordered by increasing period. *Upper panels*: T2CEPs BLHER; *bottom panels*: T2CEPs WVIR. Error bars are comparable to or smaller than the symbol size. Measurements with errors larger than 0.05 mag are not displayed. For each source we label the *Gaia* source ID and the pulsation period rounded to the last significant digit according to the error of the period determination. New discoveries by *Gaia* are flagged as such.

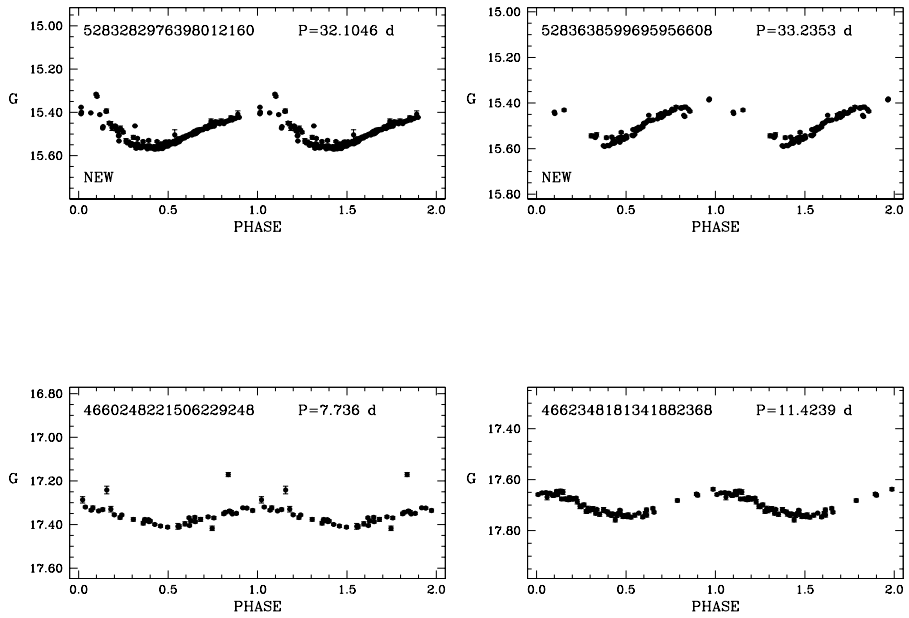

Fig. C.6. *G*-band light curves of T2CEPs released in *Gaia* DR1 ordered by increasing period. *Upper panels*: T2CEPs RVTAU; *bottom panels*: T2CEPs for which we did not identify the subtype. Error bars are comparable to or smaller than the symbol size. Measurements with errors larger than 0.05 mag are not displayed. For each source we label the *Gaia* source ID and the pulsation period rounded to the last significant digit according to the error of the period determination. New discoveries by *Gaia* are flagged as such.

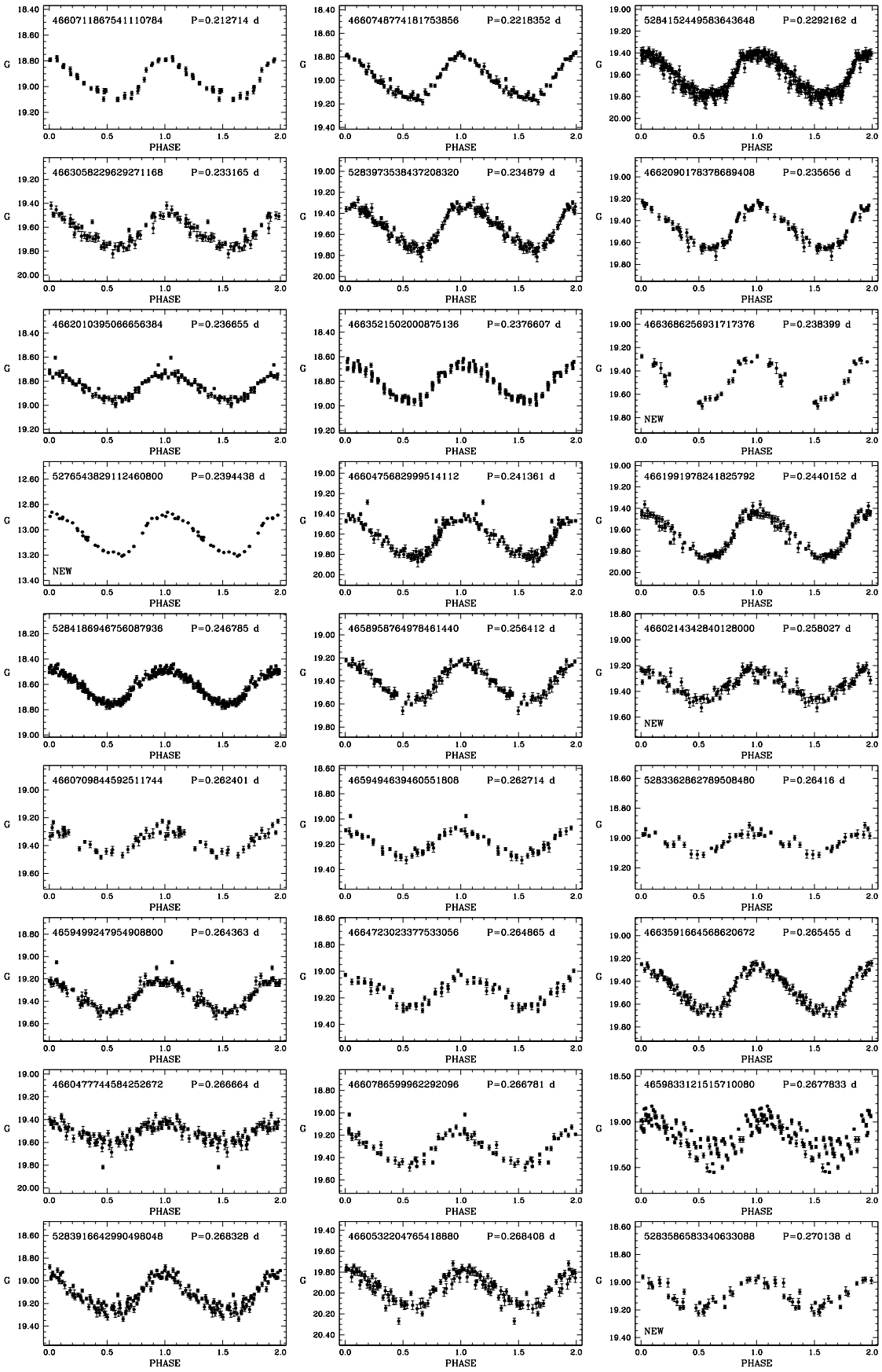

Fig. D.1. *G*-band light curves of RRc stars released in *Gaia* DR1 ordered by increasing period. Measurements with errors larger than 0.05 mag are not displayed. For each source we label the *Gaia* source ID and the pulsation period rounded to the last significant digit according to the error of the period determination. New discoveries by *Gaia* are flagged as such.

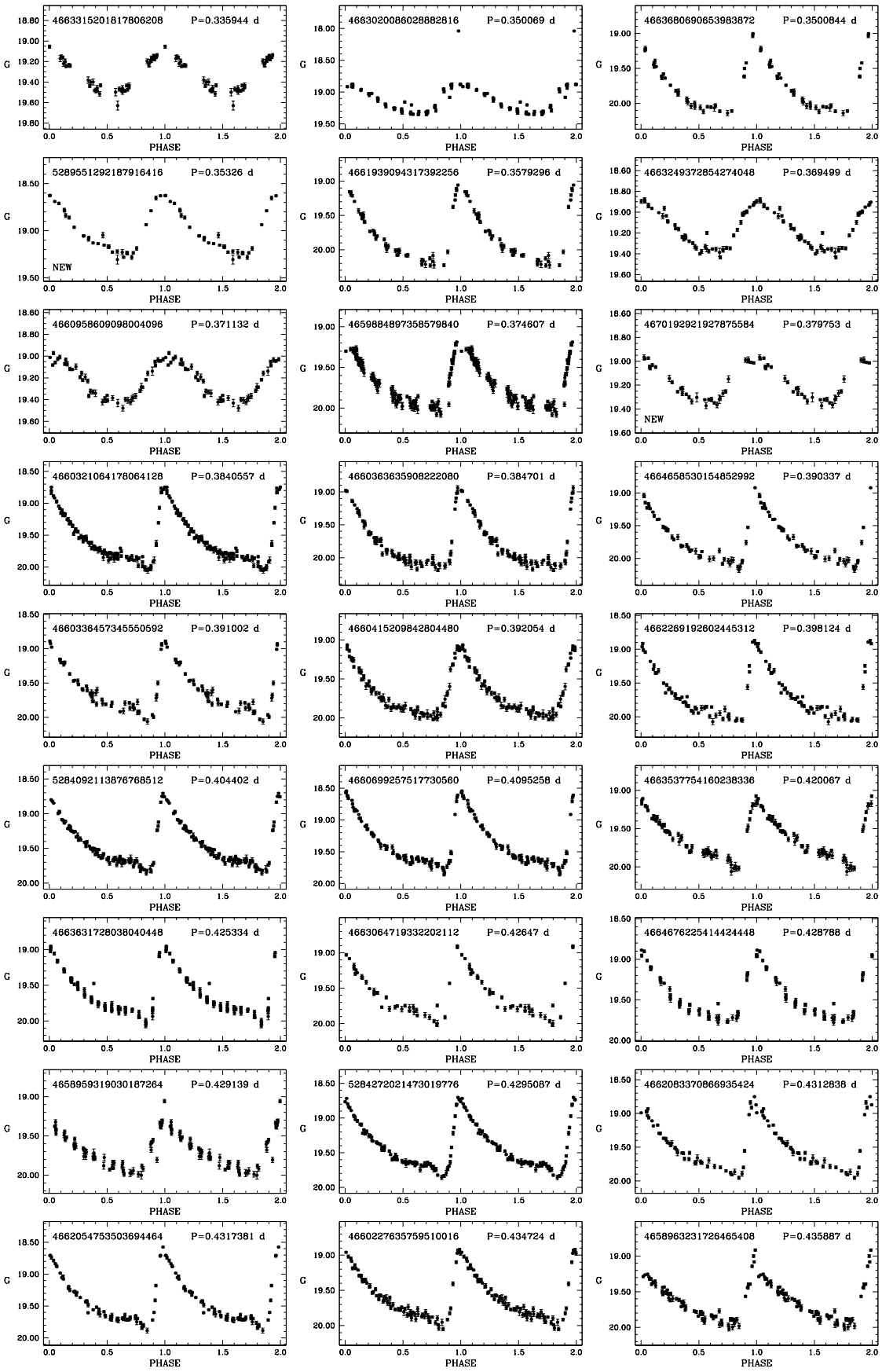

Fig. D.2. *G*-band light curves of RRab stars released in *Gaia* DR1. Sources are ordered by increasing period. Measurements with errors larger than 0.05 mag are not displayed. For each source we label the *Gaia* source ID and the pulsation period rounded to the last significant digit according to the error of the period determination. New discoveries by *Gaia* are flagged as such.